Article

Developmental Cell

Membrane Asymmetry Imposes Directionality on Lipid Droplet Emergence from the ER

Graphical Abstract

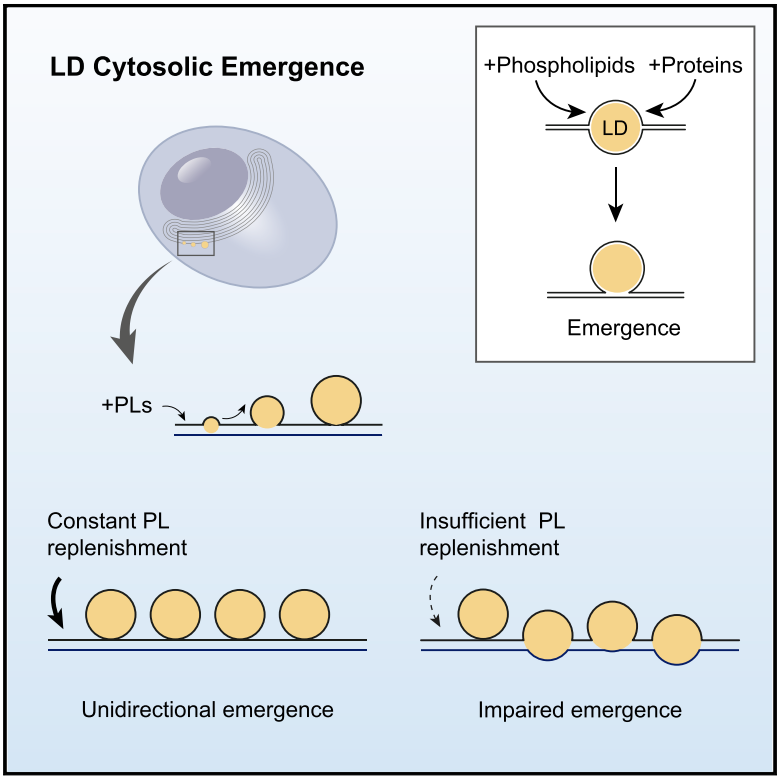

Authors

Aymeric Chorlay, Luca Monticelli, Joana Veríssimo Ferreira, ..., Mathias Beller, Pedro Carvalho, Abdou Rachid Thiam

Correspondence

thiam@ens.fr

In Brief

Lipid droplets bud from the ER into the cytosol. This directionality is crucial to lipid metabolism, but its underlying mechanism is elusive. Chorlay et al. provide evidence that it is mediated by membrane asymmetries in phospholipids and proteins. Excess phospholipids on the ER cytosolic leaflet guarantees proper lipid droplet emergence.

Highlights

- Emergence of LDs from the ER into the cytosol is facilitated by phospholipid synthesis
- Membrane imbalance in phospholipid density regulates the emergence side of model LDs
- Model LDs emerge on the side with the higher monolayer surface coverage
- Asymmetric membrane insertion of proteins regulates the emergence side of model LDs

Chorlay et al., 2019, Developmental Cell *50*, 1–18
July 1, 2019
https://doi.org/10.1016/j.devcel.2019.05.003

CellPress

Please cite this article in press as: Chorlay et al., Membrane Asymmetry Imposes Directionality on Lipid Droplet Emergence from the ER, Developmental Cell (2019), https://doi.org/10.1016/j.devcel.2019.05.003

Developmental Cell
Article

Membrane Asymmetry Imposes Directionality on Lipid Droplet Emergence from the ER

Aymeric Chorlay,[1] Luca Monticelli,[2] Joana Veríssimo Ferreira,[3] Kalthoum Ben M'barek,[1] Dalila Ajjaji,[1] Sihui Wang,[3] Errin Johnson,[3] Rainer Beck,[4] Mohyeddine Omrane,[1] Mathias Beller,[5] Pedro Carvalho,[3] and Abdou Rachid Thiam[1,6,*]
[1]Laboratoire de Physique de l'Ecole Normale Supérieure, ENS, Université PSL, CNRSSorbonne Université, Université Paris-Diderot, Sorbonne Paris Cité, Paris, France
[2]Laboratory of Molecular Microbiology and Structural Biochemistry, UMR5086 CNRS and University of Lyon, Lyon 69367, France
[3]Sir William Dunn School of Pathology, University of Oxford, Oxford, UK
[4]Heidelberg University Biochemistry Center, Heidelberg, Germany
[5]Institute for Mathematical Modeling of Biological Systems, Systems Biology of Lipid Metabolism, Heinrich Heine University, Düsseldorf, Germany
[6]Lead Contact
*Correspondence: thiam@ens.fr
https://doi.org/10.1016/j.devcel.2019.05.003

SUMMARY

During energy bursts, neutral lipids fabricated within the ER bilayer demix to form lipid droplets (LDs). LDs bud off mainly in the cytosol where they regulate metabolism and multiple biological processes. They indeed become accessible to most enzymes and can interact with other organelles. How such directional emergence is achieved remains elusive. Here, we found that this directionality is controlled by an asymmetry in monolayer surface coverage. Model LDs emerge on the membrane leaflet of higher coverage, which is improved by the insertion of proteins and phospholipids. In cells, continuous LD emergence on the cytosol would require a constant refill of phospholipids to the ER cytosolic leaflet. Consistent with this model, cells deficient in phospholipids present an increased number of LDs exposed to the ER lumen and compensate by remodeling ER shape. Our results reveal an active cooperation between phospholipids and proteins to extract LDs from ER.

INTRODUCTION

The endoplasmic reticulum (ER) is the cellular factory of lipids and membrane proteins, which are subsequently distributed to other organelles (Schwarz and Blower, 2016). This anabolic function of the ER is essential for maintaining organelle and cellular homeostasis, particularly when cells enter energy storage regimes. In these periods, excess energy is converted into neutral lipids, which upon synthesis are stored in ER-derived organelles called lipid droplets (LDs), also referred to as oil bodies or lipid bodies for plants (Martin and Parton, 2006; Murphy and Vance, 1999). The core of these droplets contains neutral lipids and is covered by a phospholipid monolayer derived from the ER bilayer, likely from its cytoplasmic leaflet (Fujimoto and Parton, 2011). Therefore, it seems essential to replenish the ER with new phospholipids to keep its integrity and proper function during lipogenesis. This is consistent with the trigger of *de novo* phospholipid synthesis by the activation of sterol regulatory element-binding protein genes in response to lipogenesis (Walker et al., 2011; Krahmer et al., 2011; Aitchison et al., 2015). These concordant events reveal a close relationship between LD biogenesis and ER homeostasis through phospholipid production (Lagace and Ridgway, 2013; Aitchison et al., 2015; Vevea et al., 2015; Ben M'barek et al., 2017) the consequences on LD biogenesis under conditions of limited phospholipid supply are poorly understood.

LDs also play important roles in several other biological processes, such as viral infections, embryonic development, and neurodegeneration (Welte, 2015). These functions are tightly related to how LDs are formed (Pol et al., 2014; Thiam and Beller, 2017; Henne et al., 2018). Neutral lipids synthesized in the ER at low concentration are likely dispersed and mobile in the space between the membrane leaflets. At elevated levels, these lipids can spontaneously demix to nucleate a lipid lens (Khandelia et al., 2010; Ben M'barek et al., 2017). The lens grows by accumulating more lipids and eventually forms a spherical LD that buds off or emerges from the bilayer (Thiam and Forêt, 2016; Pol et al., 2014; Choudhary et al., 2018). Throughout these steps toward LD maturation, proteins are dynamically targeted to the LD surface to control the LD function: they target LDs from the cytosol (Londos et al., 1995), the ER membrane (Wilfling et al., 2013, 2014; Jacquier et al., 2011), or possibly the ER lumen (Ohsaki et al., 2009). The amount of LD surface area that is in contact with the lumen and the cytosol will reflect the LD proteome and subsequent function. Most findings so far suggest that the surface of the majority of mature LDs is almost entirely exposed to the cytosol.

The emergence of LDs in the cytosol is crucial for metabolism because most regulatory proteins and enzymes that release lipids from LDs reside in the cytosol. LDs interact with nearly all cytoplasmic organelles to trade lipids and proteins (Olzmann and Carvalho, 2019). Also, they serve as a reservoir for certain

proteins such as histones during fly development (Welte, 2015) or aggregation-prone proteins that are targeted for degradation (Vevea et al., 2015). Finally, as most proteins involved in lipid secretion reside in the ER lumen, abnormal accessibility of LDs to ER luminal proteins will likely alter the secretion of very low-density lipoproteins (Ohsaki et al., 2009).

Factors controlling the directionality of LD budding are still poorly understood (Henne et al., 2018). Seipin is an integral ER protein that forms a scaffold around emerging LDs and is important for proper LD morphology (Yan et al., 2018; Sui et al., 2018). However, the depletion of Seipin does not hamper the trafficking of proteins residing on the cytosolic face of the ER, such as GPAT4, ADRP, or LiveDrop, to the LD surface (Salo et al., 2016; Wang et al., 2016). This suggests that LDs still bud toward the cytosol in the absence of Seipin, which is therefore not essential to controlling the directionality of LD budding. In contrast, depletion of fat storage-inducing transmembrane protein 2 (FIT2) results in the budding defects of an LD population (Choudhary et al., 2015). FIT2 is another integral ER membrane protein, which possibly has lipid-phosphate phosphatase activity on the ER luminal side (Becuwe et al., 2018; Hayes et al., 2017). It would transform phospholipids into diacylglycerol, which are molecules soluble in the neutral lipid phase (Thiam and Pincet, 2015). FIT2 activity would thus result in depleting phospholipids from the ER luminal leaflet. Thereupon, FIT2 generates at least transient membrane asymmetries that may determine the directionality of LD budding. Such contribution of FIT2 is appealing as a droplet in a bilayer has equivalent chances to emerge on both sides of the bilayer, unless a symmetry breaking is introduced (Chorlay and Thiam, 2018; Thiam and Forêt, 2016).

An asymmetry in phospholipid composition of the ER membrane can indeed control the directionality of LD emergence. For example, the recruitment of positively curved lipids, i.e., with bulky hydrophilic head, onto one of the monolayer leaflets will favor LD emergence toward this leaflet (Choudhary et al., 2018; Chorlay and Thiam, 2018; Zanghellini et al., 2010). Another source of asymmetry possibly modulating the direction of LD formation is membrane curvature. Curved membranes have a higher pressure in their concave region. Thus, when an LD forms, the internal pressure would tend to push the LD outside the lumen (Thiam and Forêt, 2016). The basic tubular structure of the ER membrane could hence modulate the direction of LD budding. Whether membrane curvature determines the directionality of LD emergence is not fully understood. Finally, another possible asymmetry is between the LD monolayer surface tensions (Chorlay and Thiam, 2018), which reflects an asymmetry in the surface coverage between the cytosolic and luminal monolayers surrounding LDs. Soon after nascent LDs appear in the ER (with a diameter over ~30 nm), the LD monolayer surface tension should indeed dominate spontaneous curvature and bending effects and control LD shape. In this size range, we previously worked with macroscopic model LDs and identified that an asymmetry in monolayer surface tension is sufficient to control the emergence of an artificial LD (Chorlay and Thiam, 2018).

Here, we test the hypothesis that monolayer surface-tension asymmetry is sufficient to guarantee that newly made and growing LDs become fully exposed to the cytosol. We investigate the presence of imbalances in monolayer surface tension and how they contribute to LD emergence. We find that artificial LDs, herein referred to as aLDs, emerge toward the membrane monolayer side offering better phospholipid surface coverage, i.e., having the higher phospholipid surface density and hence the lower surface tension. The monolayer coverage is also improved by the insertion of proteins; the strong binding of proteins to the aLD monolayer promotes retention of the droplet into the protein-containing reservoir. Our data support the hypothesis that systematic LD emergence toward the cytosol requires a phospholipid refill to the cytosolic leaflet of the ER membrane. Such refill ensures a good coverage (low surface tension) of this monolayer is kept. In cells experiencing a limited capacity of phospholipid supply, we observe an aberrant ER morphology concomitant with an increase in the number of LDs in large contact with the ER lumen.

RESULTS

Oil-water surface tension is diminished by covering the interface between the two liquids. In the context of LD biogenesis, the system presents two oil-water interfaces: between the neutral lipid phase and the cytosol and between the neutral lipids and the ER lumen. An asymmetry in the coverage between these interfaces will yield an asymmetry in surface tension. A monolayer surface coverage is improved by the adsorption of surfactants, which, in cells, are mainly proteins and lipids (Figure 1A). Our model predicts that the recruitment of these membrane constituents to one of the monolayers can improve this monolayer surface coating and be sufficient to promote emergence of the droplet. To test our prediction, we used the droplet-embedded vesicle system (DEV), consisting of giant unilamellar vesicles (GUVs) in which an aLD is incorporated between the leaflets of the bilayer (Figure 1B) (Chorlay and Thiam, 2018; Ben M'barek et al., 2017), mimicking the topology of an LD in the ER bilayer. We characterized the degree of emergence of an aLD from the bilayer by comparing the inner and outer surface areas of the droplet (Figure 1C). The asymmetry in the monolayer coverage, and more precisely in surface tension, is reflected by the angles formed by the droplet with the bilayer (Chorlay and Thiam, 2018), which defines the coverage asymmetry parameter (Figure 1C; STAR Methods: Determination of shape and position).

Insertion of Proteins Promotes Emergence of LDs from a Bilayer

Our model predicts that the insertion of a protein into a monolayer leaflet of an ER-enclosed LD will affect the direction of LD emergence. We tested the effect of different proteins on DEVs made with 1,2-dioleoyl-sn-glycero-3-phosphocholine (here referred to as PC) and containing triolein oil, which is the major cellular neutral lipid.

We started with Arf1, which regulates lipid metabolism and binds to cellular LDs from the cytosol (Wilfling et al., 2014; Guo et al., 2008; Thiam et al., 2013a). Arf1 uses an N-terminal myristoyl group and an N-terminal amphipathic helix to bind to membranes. These motifs are shielded within Arf1 when the protein is soluble in the cytosol and deployed when Arf1 is activated by a guanine nucleotide exchange factor and in the presence of GTP (Antonny et al., 1997); the nucleotide exchange is also promoted by reducing Mg^{2+} concentration down to the μM level by

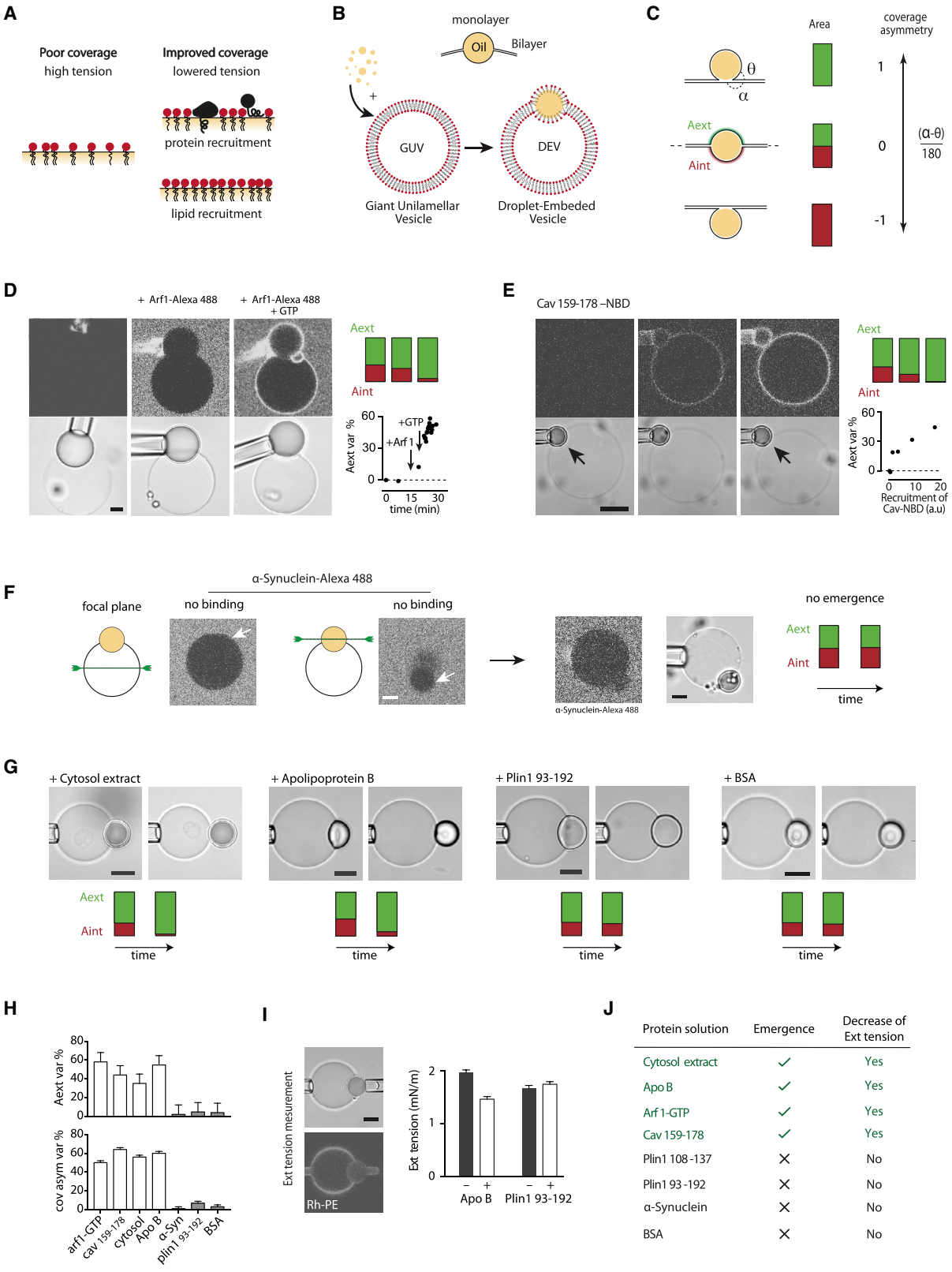

Protein solution	Emergence	Decrease of Ext tension
Cytosol extract	✓	Yes
Apo B	✓	Yes
Arf 1-GTP	✓	Yes
Cav 159-178	✓	Yes
Plin1 108 -137	×	No
Plin1 93 -192	×	No
α-Synuclein	×	No
BSA	×	No

(legend on next page)

chelating it with EDTA (Bigay et al., 2003). We can thus dynamically switch on binding and record the impact on aLD emergence. When we added Arf1-Alexa488 and EDTA to DEVs, we observed no protein recruitment, as expected (Figures 1D and S1A). Only when GTP was subsequently added, Arf1 was recruited to the membranes (Figures 1D and S1A). Recruitment of Arf1 was concomitant to the full emergence of the artificial LD to the protein solution (Figures 1D and S1B). Following Arf1 binding, the droplet outer area increased and its inner area decreased (Figure 1D). Consistent with this observation, the outer monolayer coverage was improved (Figure 1H), supporting the fact that binding induced aLD emergence by improving the monolayer coverage.

Most proteins use amphipathic helices (AHs) to associate with the LD surface. The presence of highly hydrophobic residues such as phenylalanine, tyrosine, or tryptophan, on the hydrophobic face of AHs increases membrane association. We used an AH peptide from caveolin 1 (Cav aa159-178 with an NBD tag), which binds to LDs and targets other proteins to cellular LDs (Ostermeyer et al., 2001; Kassan et al., 2013). This peptide is particularly rich in hydrophobic amino acids (Figure S1E). When it was added to DEVs, we observed an increase of the peptide signal on the DEV membrane (Figure 1E). This binding was concomitant with the emergence of the droplet into the protein solution (Figure 1E), and the improvement of the external monolayer coverage.

We next worked with an AH that lacks highly hydrophobic residues. We chose alpha-Synuclein-Alexa488, which is localized to the surface of LDs (Cole et al., 2002) but which binds *in vitro* only to droplet monolayers with poor phospholipid coating (Thiam et al., 2013a) (Figures S1C and S1F). Here, alpha-Synuclein failed to bind DEVs and the droplets did not emerge (Figure 1F); the inner and outer droplet areas remained constant and no improvement of the external monolayer coverage was detected (Figures 1F and 1H). These results suggest that only AH-containing proteins that are able to strongly associate with monolayers can promote LD emergence.

We finally investigated the effect of perilipins (Plins), which are major LD-associated proteins. Plins bind to LDs in part by using an 11-mer AH repeat (Brasaemle, 2007). To test whether this domain alone can mediate LD emergence, we examined the effect of the Plin1 11-mer AH repeat, Plin1 93–192 (Rowe et al., 2016), and a fragment of this domain also displaying an AH motif, Plin1 108–137 (Figure S1E). We found that these peptides did not enable aLD emergence (Figures 1G, 1J, and S1D). The failure of these peptides in promoting emergence is probably due to inefficient binding to a droplet monolayer, which is continuous with a phospholipid bilayer reservoir (see below). Compared to Cav 159–178 AH, the Plin fragments are less dense in hydrophobic residues (Figure S1E), which could explain (at least partly) their inefficient binding (Prévost et al., 2018). Alternatively, this Plin domain might simply require specific lipids or membrane curvature for binding; other domains of the full-length protein, or protein partners, are required to achieve the strong membrane association of the full-length protein (Ajjaji et al., 2019).

Since many proteins target LDs from the cytosol, we decided to put artificial DEVs in contact with a cytosolic extract from hepatocyte cells. We observed systematic outbound emergence of the droplets into the cytosolic medium (Figures 1G and S1D). This experimental condition closely mimics the cytosolic emergence of cellular LDs mediated by cytosolic components. Note the small decrease of the GUV size because of water evaporation (Figure 1G); this decrease only affects the bilayer tension and does not introduce membrane asymmetry (Chorlay and Thiam, 2018).

Figure 1. The Insertion of Proteins Promotes Artificial LD Emergence

(A) The surface tension of an oil-water interface is decreased by improving the surface coverage with surfactants, such as proteins and phospholipids.

(B) Top: schematic of an artificial LD (aLD) embedded in a bilayer as during LD formation. Bottom: principle of the droplet-embedded vesicle (DEV) system, made by an aLD incorporated into the intermonolayer space of a giant unilamellar vesicle (GUV).

(C) LD emergence is characterized by the fraction of its external and internal surface areas. The imbalance of monolayer tension between the interior and exterior, reflecting the asymmetry in surface coverage, defines the coverage of the asymmetry parameter (see STAR Methods).

(D) Arf1 binding to DEVs promotes artificial LD extraction. Left: a PC DEV with a triolein droplet is made and Arf1-Alexa488 added to the external medium. Arf1 DEV-recruitment occurred only with the subsequent addition of GTP. The artificial LD emerged toward the exterior upon Arf1 binding. The glass pipette was used for softly maintaining the DEV under the observatory region during injection; the pipette was motionless and images were rotated for visualization. Top right: external and internal surface areas corresponding to the pictures shown on the left. Bottom right: corresponding time course displaying the protein recruitment effect on the external Area ("Aext var" represent the external area variation). Arf1 recruitment on the bilayer and droplet surface is displayed in Figure S1A. Additional images of fully emerged aLDs following Arf1 binding are displayed in Figure S1B. Scale bar, 10 μm.

(E) The fragment of caveolin 159–178, used in the Hpos construct, which targets LDs (Kassan et al., 2013), bound to DEVs and promoted aLD extraction. Left: Cav 159–178-NBD was added to the medium of a PC DEV containing triolein droplets. The artificial LD emerged toward the exterior upon Cav159-178-NBD binding. The glass pipette was used for softly maintaining the DEV under the observatory region during injection. Top right: external and internal surface areas corresponding to the pictures shown on the left. Bottom right: effect of Cav 159–178-NBD recruitment on artificial LD external Area. ("Aext var" represent the external area variation). Scale bar, 10 μm.

(F) Alpha-Synuclein did not bind to PC DEV (left), even after 30 min (right), and the artificial LD did not emerge. Arrows point to the GUV and droplet interface. The external area did not vary. Scale bars, 10 μm.

(G) A cytosolic extract from Huh7.5 cells and apolipoprotein B promoted artificial LD emergence from DEVs, while Plin1 93–192 or BSA did not. Corresponding external and internal surface areas variation are shown below each condition. For fluorescence confocal micrographs see Figure S1D. For each of these conditions, external area variation and coverage asymmetry is displayed over time in Figure S1D. Scale bars, 10 μm.

(H) The induced effects of the proteins on the aLD external surface area variation (top) and coverage asymmetry (bottom) are displayed. Error bars are measurement precision.

(I) The external monolayer tension of the artificial LD is measured by microaspiration technique (left images—fluorescent signal is rhodamine-PE (Rh-PE)), before and after addition of apolipoprotein B and Plin1 93–192. A decrease of tension was measured when apolipoprotein B was added, while tension remained constant with Plin1 93–192. Scale bar, 10 μm; error bars are measurement precision.

(J) Summary of the effect of the protein solutions on aLD emergence and membrane coverage asymmetry (decrease of external surface tension).

See also Figure S1.

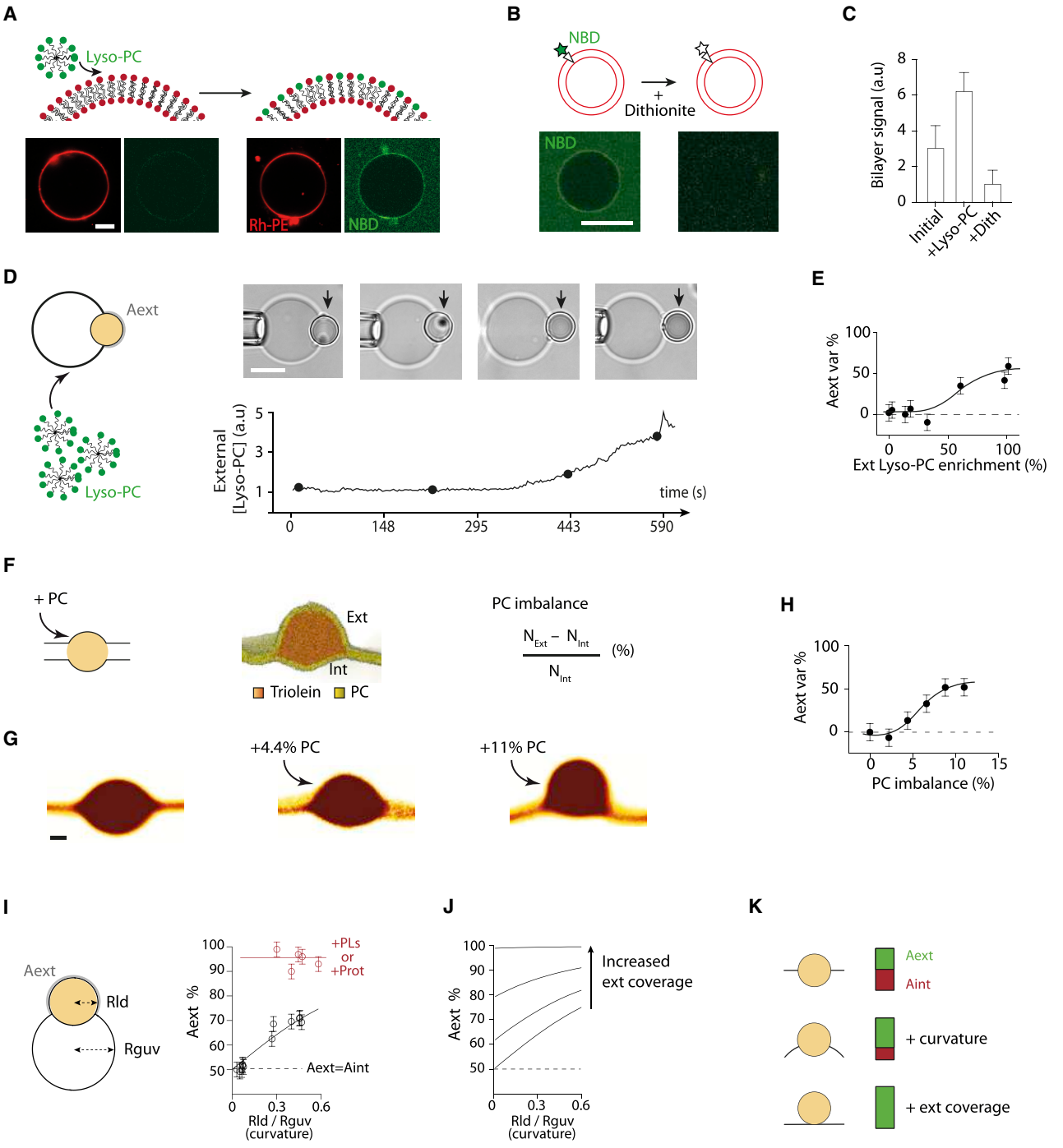

Figure 2. Artificial LDs Emerge toward the Monolayer Bearing Excess Phospholipids

(A) A Lyso-PC micellar solution containing NBD-PE (1% w/w to lyso-PC) was added to GUVs marked by Rhodamine-PE (Rh-PE) (0.5% w/w to PC). Lyso-PC molecules, reported by NBD, are recruited to the external GUV surface see arrows (and Figures S2B and S2C). Scale bar, 10 μm.

(B) Determination of the location of recruited lyso-PC molecules by following NBD-PE signal. Dithionite, an NBD quencher, is added to the external solution. The NBD signal disappears entirely, suggesting that lyso-PC enrichment occurred only on the external leaflet. Scale bar, 10 μm.

(C) Relative NBD signal on the bilayer displayed for different GUVs: before any treatment, after Lyso-PC micelle addition, and after dithionite treatment. Data are represented as mean ±SD.

(D) A Lyso-PC micellar solution containing NBD-PE was added to a DEV. When the NBD concentration around the DEV increased (see example in Figure S2B), the embedded droplet emerged toward the exterior. Scale bar, 10 μm.

(E) The droplet external area variation in (D) is displayed as function of the Lyso-PC enrichement on the DEV, which is reported by the NBD-PE signal. Error bars are measurement precision.

(F) Simulated situation with increasing the number of PC molecules in the external leaflet of a bilayer containing a 35 nm-sized triolein droplet.

(legend continued on next page)

To further challenge our hypothesis, we tested the effect of the addition of apolipoprotein B (ApoB) on LD emergence. ApoB is localized in the ER lumen where it was shown to retain LDs following lipid accumulation (Ohsaki et al., 2008). Here, we indeed found that the addition of ApoB promoted aLD emergence (Figures 1G and S1D) toward the ApoB-containing medium. In cells, ApoB would thus promote the emergence of LDs into the ER lumen. As a control, we finally also tested for an effect of bovine serum albumin, which is not an LD protein and observed no emergence (Figure 1F).

These observations support our hypothesis that the insertion of proteins in an LD monolayer promotes LD emergence by decreasing the monolayer surface tension, through improving its surface coverage. To confirm the link between protein binding and surface tension, for selected examples, we measured the changes in surface tension upon addition of the protein using the micropipette aspiration technique (Figure 1G). Upon addition of ApoB (which improved the monolayer coverage and induced aLD emergence) (Figures 1H and S1D), we observed a decrease in the surface tension of the external monolayer (Figure 1I); on the contrary, in the case of Plin1 93–192 (or proteins which did not induce budding), no change in the external tension was measured (Figure 1I). Emergence of aLDs induced by protein binding is therefore mediated by the decrease in monolayer tension (Figure 1J).

In summary, the asymmetric insertion of proteins to an aLD surface promotes emergence toward the protein-enriched monolayer. This emergence results from a decrease of this monolayer surface tension due to an improvement of its surface coverage. In cells, controlling LD emergence would require regulating the access of proteins to the luminal and cytosolic sides of nascent LDs. Overexpression of proteins that strongly bind to LDs from these compartments will affect LD emergence.

Lipid Droplets Emerge toward the Membrane Monolayer Side Bearing an Excess of Phospholipids

Monolayer surface coverage can also be improved by increasing the surface density of phospholipids (Figure 1A). Phospholipids can be expected to be more effective than proteins at decreasing tension, by virtue of their higher flexibility and ability to form well-packed interfaces. For example, we measured the minimal surface tension reachable in a monolayer made of PC and found that it is lower than that obtained with ApoB, or with previously studied proteins (Figure S2A). This analysis suggests that the monolayer coverage can be improved more effectively by adding phospholipids than by inserting proteins. The addition of phospholipids could thus be more effective at promoting LD emergence.

We decided to asymmetrically increase the number of phospholipids in DEVs, for which the outer monolayer is more accessible. However, increasing the number of PC molecules by direct supply is difficult because PC forms in solution relatively stable and non-fusogenic bilayer structures. Instead, we chose to test the addition of Lyso-PC because it forms micelles, which spontaneously adsorb onto membranes. To prove this idea, we first made Lyso-PC micelles containing fluorescent NBD-PE (1%, w/w) and added them to PC GUVs (Figure 2A). Over time, after the micelles arrived in the vicinity of the GUVs, the phospholipids were recruited to the membrane as reported by the increase of the NBD signal (Figures 2A, 2C, and S2B). To know whether the phospholipids were only recruited to the external monolayer, we added dithionite to the bulk solution. Dithionite quenches the NBD signal and can only access the outer leaflet of the GUV, as it does not cross the membrane (Laouini et al., 2012). After few minutes, the NDB signal disappeared completely (Figures 2B, 2C, and S2C), supporting that phospholipids were mainly recruited to the external GUV monolayer. We hence decided to use this technique to increase the number of phospholipids in the outer monolayer of DEVs.

We took DEVs in which the aLD monolayers had no asymmetry in phospholipid composition. We next added Lyso-PC micelles to increase the number of phospholipids in the outer monolayer surface. We systematically observed that the aLDs emerged toward the outside (Figures 2D and 2E), exactly as with the insertion of proteins. This observation confirmed that the aLD emergence happens on the monolayer with the better surface coverage, mediated here by a phospholipid supply from the bulk solution.

It is worth noting that Lyso-PC has a positive spontaneous curvature, which, in principle, can have an effect on LD emergence at nanometric scales, as recently proposed (Choudhary et al., 2018). However, in our macroscopic scale (Figure 2D), spontaneous curvature effects should be dominated by surface tension (Thiam and Forêt, 2016). We hypothesize that the aLD emergence observed here is not due to Lyso-PC positive curvature but to its ability to improve the external monolayer surface coverage. To demonstrate that the asymmetry in monolayer phospholipid coverage is the main factor that mediates emergence, we used molecular dynamics simulations. Compared to experiments, in simulations it is much easier to increase or decrease the amount of phospholipid selectively in each leaflet. We performed simulations of phospholipid bilayers exclusively made of PC (~75 nm lateral size) and bearing a ~35 nm-sized triolein droplet (Figure 2F); note that PC has a slightly negative spontaneous curvature (Zimmerberg and Kozlov, 2006), opposite to the pronounced positive curvature of Lyso-PC. Starting

(G) Examples of cross sections of multiple merged snapshots of the results for different PC imbalances (0%, 4.4%, and 11% PC excess in upper leaflet). See Figure S2D for more examples. Scale bar, 7 nm.

(H) The aLD external area variation in (G) shows the externalization of the droplet with increased PC imbalance. Related to Figure S2D. Error bars are measurement precision.

(I) The external area fraction of aLDs in a DEV is displayed against the aLD radius over the GUV radius (Rld/Rguv), which takes into account the bilayer curvature. Red, values for experiments where phospholipids or proteins (that bound were added to the external medium) and black, no addition of materials. Error bars are measurement precision.

(J) Simulated relative aLD external area versus Rld/Rguv with varying the coverage asymmetry (0, 0.2, 0.6, and 0.98).

(K) On a flat and finite bilayer a large droplet will be in the middle of the bilayer, with external and internal areas being equal (top); curvature of the bilayer will induce only partial emergence (middle); providing phospholipids to increase the coverage asymmetry alone (bottom) is sufficient to promote full emergence.

See also Figure S2.

from a completely symmetric system (equal number of PC molecules on both leaflets), we performed simulations with an increasing phospholipid imbalance, up to 11% excess of PC molecules in the upper monolayer (Figures 2G and S2D). We observed that a 4% imbalance in the phospholipid count is sufficient to induce a significant asymmetry in droplet shape. The asymmetry grows as the lipid imbalance increases, and it causes the aLD to emerge toward the PC-enriched monolayer (Figures 2G, 2H, and S2D). These results show that LDs can emerge from the ER bilayer simply by maintaining an excess of phospholipids on one monolayer side, without using phospholipids with positive spontaneous curvature, which fully agrees with our *in vitro* data (Figures 2A–2E).

It is important to note that generation of high membrane coverage asymmetry cannot be maintained in the bilayer, as it would otherwise destabilize the membrane both *in vitro* and *in silico*. Instead, the surplus of phospholipids is absorbed by the increasing surface of the emerging droplet. This process is almost instantaneous as it happens in much less than a second, based on our previous work (Chorlay and Thiam, 2018). During LD budding *in vivo*, possible lipid flipping, which happens over minutes (Pomorski and Menon, 2006) would probably not be fast enough to reset the bilayer symmetry (see STAR Methods: Time scale of LD emergence).

Membrane Curvature Facilitates Lipid Droplet Budding but a Supplement of Phospholipids Remains Essential to Guarantee Full Emergence

The ER consists of relatively flat cisternae and high curvature tubules, with diameters in the range of 30–100 nm (West et al., 2011). The DEV system does not fully capture the shape nor the scale of such tubules; also, because of the large size of DEVs, the effect of membrane rigidity on LD shape is supposed to be negligible. Nonetheless, by conserving droplet-to-membrane aspect ratios, our DEV system can be seen as an upscale of a section of an LD forming on a tube (Figure 2I, left). We thus decided to use it to explore possible contributions of bilayer membrane curvature on LD emergence.

We made DEVs presenting various droplet-to-GUV aspect ratios by varying the aLD and GUV sizes. For each case, we measured the fraction of the droplet area exposed to the exterior (A_{ext}). This surface fraction was represented against the ratio of the droplet-to-GUV size (Figure 2I), which merely represents the curvature of the GUV bilayer membrane relative to the droplet. Droplets that were small relative to the GUV size were equally exposed to both membrane sides, $A_{ext} = A_{int} = 50\%$ (Figure 2I, lower black circles). In contrast, larger droplets had an external area larger than the inner area, $A_{ext} > 50\%$, indicating that they emerged more toward the exterior (Figure 2I, upper black circles). These results suggest that membrane curvature favors the outward emergence of large droplets. However, we never observed full emergence of large droplets in the DEVs, i.e., $A_{ext} = 100\%$, unless phospholipids or proteins were added to the external leaflet (Figure 2I, red circles). This suggests that curvature promotes outward budding, but the addition of phospholipids to the external leaflet is necessary to guarantee full emergence.

To further understand our data, we used a basic theoretical model computing the balance of forces acting on a droplet in a bilayer (Chorlay and Thiam, 2018) (STAR Methods: Determination of shape and position). This model fitted well with our experimental data (Figure 2I, black line), which confirmed that the effect of phospholipid surface density is stronger than the effect of curvature in determining the direction of emergence (Figures 2J, 2K, S2E, and S2F). It is worth noting that if no phospholipid is added in the system, the externalization of growing droplets would induce stretching of the external monolayer. This monolayer, not supplemented with phospholipids, would reach a lower coverage (higher surface tension) than the inner one, which, in turn, would promote inward budding (Figure S2G). In this situation, the droplets will tend to remain in contact with the lumen despite the effect of curvature.

In conclusion, our data suggest that when an LD forms and grows, the ER membrane curvature helps to preset the direction of emergence of the LD, i.e., in the cytosol. However, the supplement of phospholipids, and eventually of proteins, to the cytosolic monolayer would be required and be more efficient at promoting the full emergence of the LD into the cytosol. In case of phospholipid deficiency on this leaflet, droplets would fail to properly emerge and remain in contact with the ER lumen (Figure S2G).

Altogether, our results in Figures 1 and 2 suggest that in close systems, i.e., where there is no excess or addition of phospholipids or proteins, the droplet emergence essentially follows leaflet asymmetry. Emergence occurs toward the monolayer with the better surface coverage, which is improved by the insertion of proteins and phospholipids. In open systems, such as in cells, the order of events is not known, so asymmetry in leaflet coverage may be induced by multiple events. In any case, our *in vitro* observations predict that LD exclusive formation into the cytosol requires a regulation of phospholipid density and protein binding in of each monolayer.

Stimulated LD Production in *Saccharomyces cerevisiae* Cells by Oleic Acid Is Associated with Aberrant ER Morphology

Under basal conditions, the ER cytosolic side probably has enough proteins and phospholipids to impose directionality on LD budding. However, during high lipogenesis regimes, the demands for LD surface coating may become limiting. The emergence of many LDs will deplete phospholipids from the cytosolic leaflet of the ER membrane. In this case, if phospholipids are not present in large excess, quickly replenished, or replaced by other surfactant molecules (e.g., proteins), LD emergence (Figure S2G) and ER morphology could both be affected.

We considered cellular model systems in which the ER membrane surface can be easily visualized and characterized. We chose to work with the *Saccharomyces cerevisiae* cells because most of their ER surface is essentially composed of two domains, the cortical and nuclear ER (West et al., 2011). The total apparent surface of these two-ER domains can be approximately determined by considering them as spherical surfaces, which is an overestimation of the ER surface based on quantifications from 3D ultrastructure imaging (Wei et al., 2012). We reasoned that if too many LDs were to form in these cells, they would mobilize phospholipids from the ER cytosolic leaflet and the ER membrane might find a way to compensate for this asymmetric usage of phospholipids.

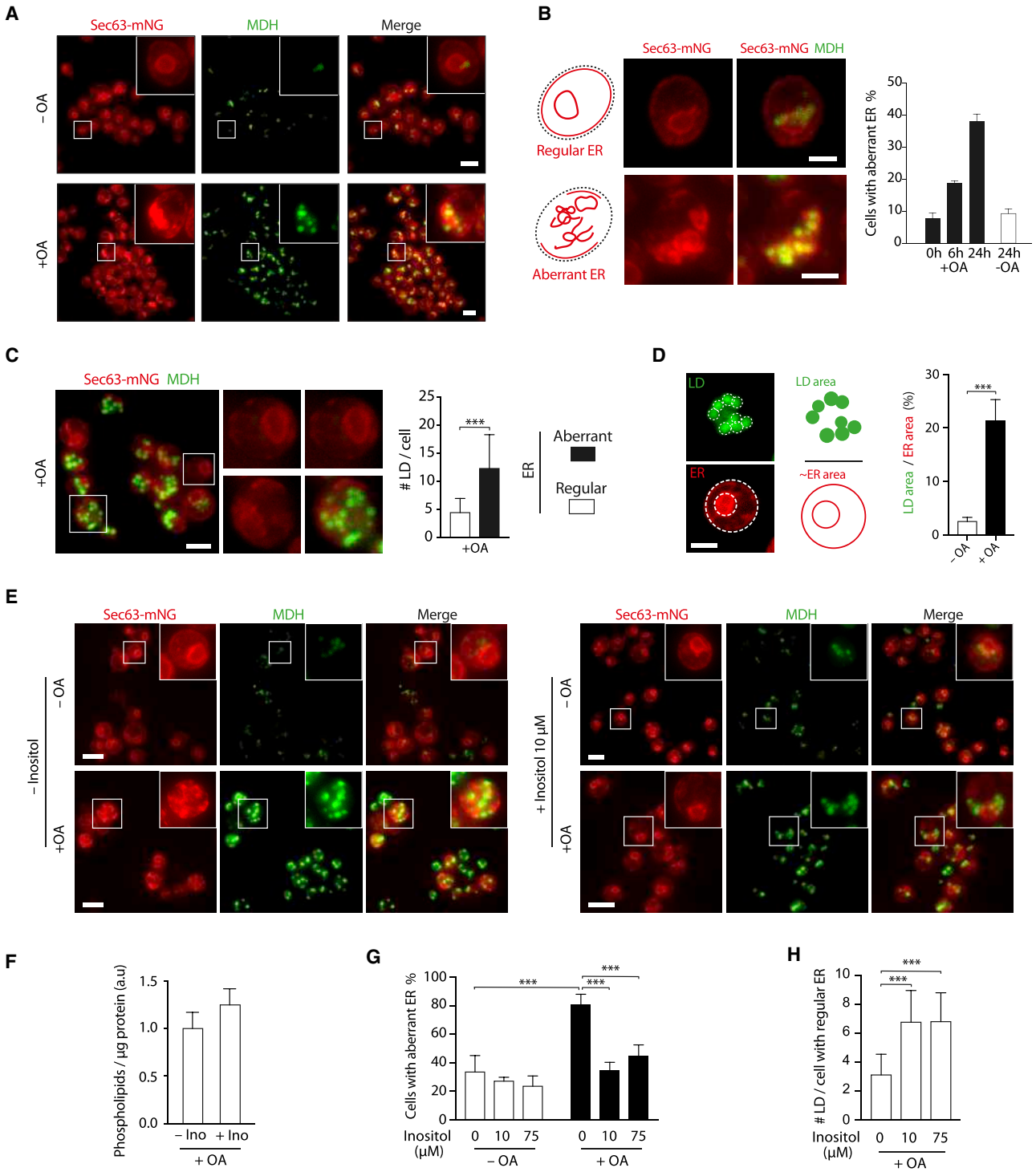

Figure 3. Boosted LD Formation Is Concomitant with Remodeled ER Morphology

(A) Representative images of wild-type (WT) *Saccharomyces cerevisiae* cells in stationary phase, imaged after 24 h, with or without treatment with oleic acid (OA). The ER marker protein, Sec63, was endogenously tagged with monomeric NeonGreen (Sec63-mNG) and LDs were labeled by monodansylpentane (MDH). Images shown represent z projection of different confocal planes. Scale bar, 5 µm.

(B) Left: schematics and representative images of cells with regular or aberrant ER. An image is shown for each situation. Images shown represent z projection of different confocal planes (shown in Figure S3F) Scale bar, 2 µm. Right: Quantification of the number of cells with aberrant ER, 0, 6, and 24 h after OA treatment of cells in log phase. Control cells with no OA addition are shown at 24 h time point. n > 200 cells/condition (ntotal = 1,276). Data are represented as mean ±SD. See Figures S3A–S3C for other tested conditions.

(legend continued on next page)

Yeast strains expressing the ER marker protein Sec63 at endogenous levels, tagged with the monomeric fluorescent protein neon green (Sec63-mNG), were grown in oleate-containing media (0.1%) for 6 to 24h, in order to produce numerous and big enough LDs to quantify by fluorescence (LDs were stained by monodansylpentane, MDH). Under these conditions, we observed increased numbers of cells with aberrant ER membranes, as compared to non-oleate loaded cells (Figures 3A and 3B). Unusual ER membrane signals appeared in the cytoplasm in the form of lumps or threads. The cortical ER, which seemed to be discontinuous or disappeared, was more affected than the nuclear ER, which was sometimes shrunk or distorted (Figures 3B and S3F). These phenotypes were observed irrespective of whether LD production was stimulated during exponential or stationary phases (Figures S3A and S3D). Interestingly, cells with aberrant ER very often contained larger numbers of LDs (Figures 3C and S3E), suggestive of a link between the LD number, or total LD surface, and ER morphology defects. By estimating the amount of total LD surface over the cortical and nuclear ER surface, we found that this ratio was less than 2% in most cells cultured in regular media (no oleate) (Figure 3D)—consistent with values from tomogram reconstitution data of *Saccharomyces cerevisiae* cells (Wei et al., 2012; West et al., 2011). In contrast, in cells grown in oleate-containing media, this ratio was more than 22% (Figure 3D).

Assuming that the LDs were all formed toward the cytosol in the oleate-loaded cells, the ER membrane would be depleted of 22% in phospholipids on its cytosolic leaflet, which would generate a huge asymmetry on the membrane. Indeed, a pure bilayer can only withstand an asymmetry of less than 1% in phospholipids (Segrest et al., 2015; Farge and Devaux, 1992). Otherwise, the membrane will undergo spontaneous reshaping to release the stress created by this asymmetry (Segrest et al., 2015; Farge and Devaux, 1992). With the potential membrane asymmetry of 22% induced by LD formation, such spontaneous membrane reshaping mechanism could explain, at least in part, the observed loss of the normal ER morphology.

Phospholipids may be refilled to the ER cytosolic leaflet during the formation of LDs in non-fed cells, through the activity of scramblases (Pomorski and Menon, 2016). In contrast, the fed cells were probably challenged beyond their capacity of phospholipid supply for covering the LDs. Thus, they would likely respond to this demand by remodeling their ER membrane. Consistent with this analysis, cells fed under our working conditions were previously reported to reach a ~1.3-fold increase of their total phospholipid (Grillitsch et al., 2011). Our quantifications from thin-layer chromatography showed that the total phospholipid level barely changed (Figure S3G). Overall, these observations suggest that LD formation in oleate feeding conditions, the phospholipid levels were not sufficient to overcome the demand.

We reasoned that increasing phospholipid production under lipogenic conditions would rescue the aberrant ER phenotype. In yeast, inositol is a major component regulating phospholipid biosynthesis (Carman and Henry, 1989). It is a precursor of the synthesis of PI, a main lipid of yeast ER membranes. The enzymes executing PI synthesis are located on the cytosolic membrane side of the ER (Carman and Henry, 1989). The addition of inositol to yeast cells led to a 5-fold increase in PI as well as overall cellular phospholipid levels (Gaspar et al., 2006) (Figure S3H); only PC levels were slightly decreased, as reported before (Gaspar et al., 2006) (Figure S3H). We cultured yeast cells in the presence of oleate and inositol and quantified the amount of total phospholipid per microgram of proteins. The overall phospholipid level was increased by ~30% (Figure 3F) and we found a significant increase of PI (Figure S3H). Interestingly, we found that the addition of inositol rescued the aberrant ER phenotype (Figures 3E and 3G). In this condition, we also noticed that cells presenting a normal ER morphology tolerated a higher number of LDs than the control cells, i.e., without inositol addition but in the presence of oleic acid (OA) (Figure 3H). Based on our model, these observations suggest that the cells treated with inositol, which induced an increase in total phospholipids, were better set with phospholipids to cover the total surface of generated LDs. This overall rescue of the aberrant ER phenotype is probably mediated by the presence on the ER cytosolic monolayer of additional phospholipids, probably PI (Figure S3H), which contributed to the coverage of the LDs.

Finally, we tried to accentuate the aberrant ER phenotype, by aiming at decreasing the number of phospholipids available in the cell. We deleted the choline-phosphate cytidylyltransferase gene (PCT1), the rate-limiting enzyme in the Kennedy pathway of PC biosynthesis (Dowd et al., 2001). However, no striking differences were observed between WT and pct1Δ, except at 6 h after OA treatment where pct1Δ cells showed a stronger increase of aberrant ER frequency (Figure S3D). This is probably because the large asymmetric phospholipid usage introduced by the numerous LDs formed was already too strong, and therefore no further ER membrane reorganization could be induced. As an alternative, the contribution of PCT1 to PC synthesis under our working condition could be smaller than pathways involving e.g., Cho2 and Opi3.

(C) Cells with the aberrant ER phenotype statistically contained more LDs than cells with a normal ER. t test ($p < 0.0001$), n = 140 cells, data are represented as mean ±SD. Similar results for *pct1*Δ are presented in Figure S3E. Scale bar, 5 μm.

(D) Left: illustrative image showing the measuring principle of total LD area and cortical and nuclear ER surface. Scale bar, 2 μm. Right, quantification of the total LD over ER area at 24 h in stationary phase with and without oleate. t test show a significant difference ($p < 0.0001$); n = 10 cells. Data are represented as mean ±SD.

(E) Left: representative images of cells in stationary phase, imaged after 24 h, with or without with (OA). Right: the cells were additionally treated with 10 μM inositol. Scale bars, 5 μm.

(F) Total amount of phospholipids/μg of proteins in the presence of OA, with and without inositol treatment. Quantification of thin-layer chromatography (Figure S3H). Experiment was repeated three times. Data are represented as mean ±SD.

(G) Quantification of the number of cells with aberrant ER at 24 h for various inositol concentrations, with and without OA treatment (conditions displayed in E). n > 200 cells/condition (ntotal = 1,979). t test show significative diferences with ($p < 0.001$). Data are represented as mean ±SD.

(H) Cells presenting a normal ER statistically bear more LDs in inositol treatment. n = 30 cells ($p < 0.0001$), data are represented as mean ±SD.

See also Figure S3.

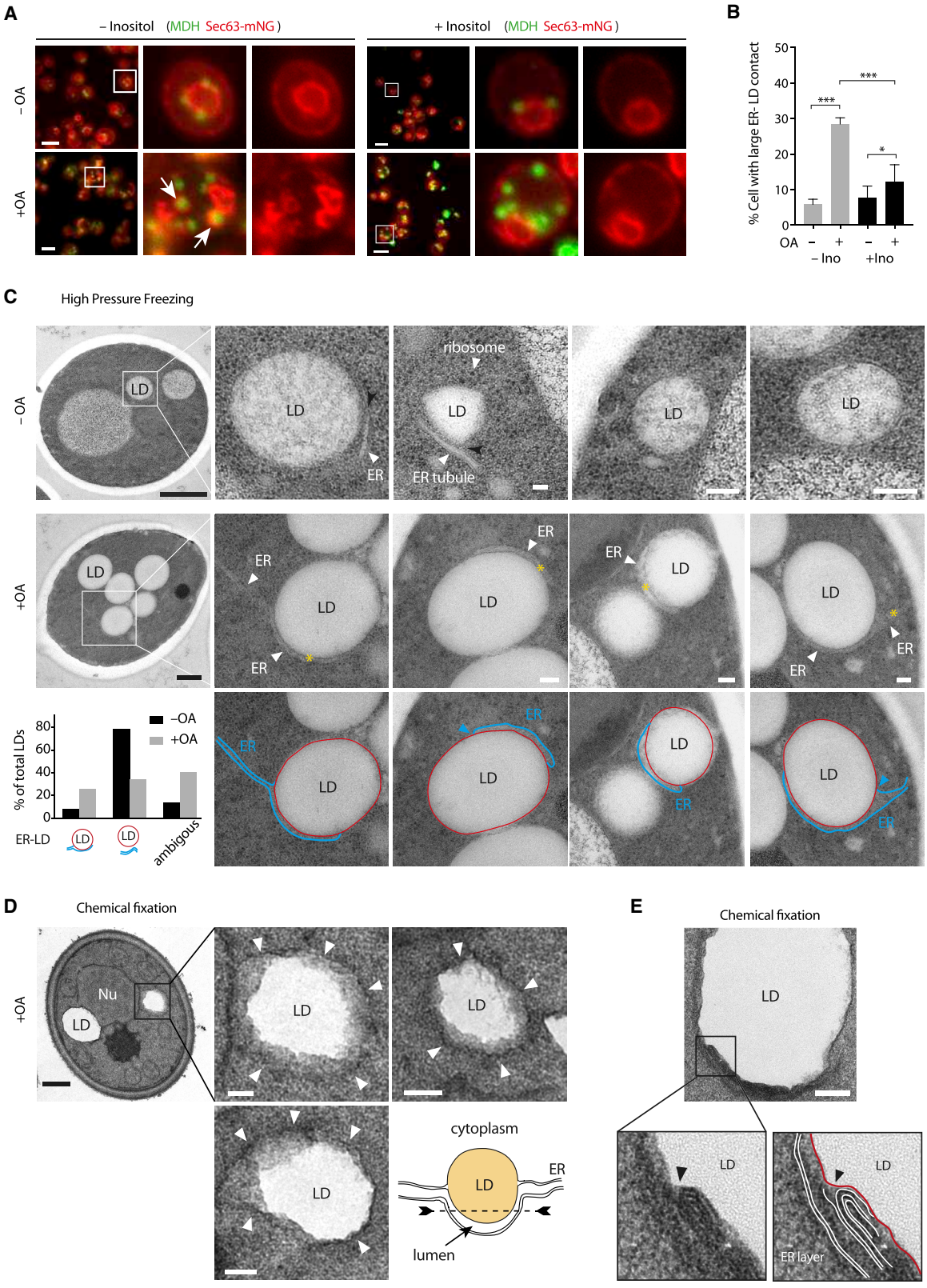

Figure 4. LD Proper Emergence in *Saccharomyces cerevisiae* Is Facilitated by Phospholipid Production

(A) *Saccharomyces cerevisiae* cells in logarithmic growth phase treated with OA show LDs with large contact zones with the ER membrane (white arrows). Less LD-ER contact zones were observed after inositol treatment, as in non-oleated cells. Sec63-mNG marks ER and LD are MDH stained. Scale bar, 5 μm.

(legend continued on next page)

In summary, the formation of multiple LDs correlated with the appearance of an aberrant ER membrane. This phenotype was rescued by the addition of inositol, which led to an increase in phospholipid levels. These results show that increasing phospholipid levels during lipogenesis ensures the formation of multiple LDs in the cytosol and keeping the ER morphology intact.

Proper LD Emergence Is Facilitated by Phospholipid Synthesis in Yeast Cells

The formation of multiple LDs depletes phospholipids from the cytosolic leaflet of the ER membrane. If the ER cannot meet this phospholipid demand on the cytosolic monolayer its luminal monolayer could become better covered with phospholipids, at least transiently. Therefore, we expect that in such conditions some LDs fail to fully emerge in the cytosol and instead, remain in contact with the ER lumen.

In the yeast cells fed with oleate to stimulate LD production, we observed increased numbers of LDs sharing large contacts with the ER membrane marker (Figure 4A, left and Figure 4B). This phenotype was much more pronounced in cells with an aberrant ER. In these cells, the ER sometimes adopted a cup shape structure, which embedded the LD or surrounded the LD on the observed plane (Figure 4A, arrows). This phenotype was more pronounced in *pct1Δ* cells (Figure S4A). Note that these LDs were not in the nucleus, which remained intact in most cases (Figures 4A, S4A, and S4B). These data support a failure in LD emergence in the cytosol, which would be consistent with our model of the need of phospholipid refill on the cytosolic monolayer for proper LD emergence (Figure 2). In fact, by the addition of inositol, which increased phospholipid levels and reduced the aberrant ER phenotype (Figures 3E–3G), we found that the fraction of LDs which were in large contact with the ER membrane was significantly decreased (Figure 4A, right and Figure 4B).

To visualize the topology of the ER-associated LDs, we performed electron microscopy (EM) imaging of high-pressure frozen (HPF) cells. In control (non-oleate-loaded) cells, most LDs were not in large contact with the ER (Figure 4C, top). Even though the ER membrane was sometimes close to LDs in these cells, there was a perfectly distinguishable free space between the two organelles (Figure 4C, top, black arrowhead). In oleate-loaded cells, which developed an aberrant ER phenotype, LDs were larger than in control cells and were often molded by ER membranes (Figure 4C). The ER lumen, marked by a membrane region devoid of ribosomes, seemed to be in contact with the LDs. In some cases, the focal section enabled us to catch structures that looked like an unzipping of the ER bilayer at the LD edge (see Figure 4C, blue arrowhead). These phenotypes might look like mere membrane wrapping phenomena but rather could be the signature of a defect in LD emergence, as theoretically predicted (Figure S2G). This conclusion is consistent with previous studies, performed exactly under our working conditions, which showed that the LDs were accessible to proteins expressed in the ER lumen, by both fluorescence and EM imaging (Mishra et al., 2016). To better visualize the membrane, we opted for a chemical fixation of the cells instead of HPF. With this method, membranes were better labeled and darker (Figure 4D, white arrowhead and Figure S4C). This approach enabled us to identify section planes where LDs were in contact with the ER lumen in oleate-loaded cells, as previously seen in yeast cells lacking FIT2 (Choudhary et al., 2015, 2018). On other focal sections, we also observed phenotypes where the ER membrane formed stacks on a portion of the LDs (Figures 4E and S4D), and sometimes we could catch what seemed to be an unzipping of the membrane at the LD edge (Figure 4E, black arrowhead).

LDs Remain More in Contact with the ER in *Drosophila* Cells with Reduced CCT1 Activity

We decided to test our model in a different cell type by manipulating phospholipid levels. We worked with *Drosophila* Kc167 cells because the synthesis of PC in these cells essentially happens through the Kennedy pathway. Contrary to PCT1 inhibition in yeast, PC level in *Drosophila* cells is markedly reduced by inhibiting the rate-limiting enzyme in PC synthesis, the cholinephosphate cytidylyltransferase enzyme 1 (CCT1) (Krahmer et al., 2011; Aitchison et al., 2015). Cells expressing the GFP-tagged ER marker Sec61β were treated with dsRNA targeting the CCT1 encoding transcript (Figure S5A) and then they were fed with oleate. We observed an increase in the number of large LDs (Figures S5C and S5D), a signature of PC deficiency in CCT1 depletion (Krahmer et al., 2011; Aitchison et al., 2015). As compared to yeast cells, in the fly cells the ER formed a complex 3D network, which was a limitation to properly characterize ER membrane morphology and to quantify the LD-to-ER surface ratio. Nonetheless, by using super-resolution structured illumination microscopy, in the CCT1-depleted cells, we found LD phenotypes similar to the ones found in yeast (Figures 4A, 4C, 4D, S4A, and S4C): as compared to WT control cells, many LDs were much more often in close contact with the ER membrane marker (Figure 5A), as visualized through z stacks. For many LDs, there were focal planes where the ER membrane marker protein was extremely close to the LD surface (Figure 5A,

(B) Quantification of the number of cells presenting large ER-LD contact (with or without inositol (10 μM)): ER-LD contact is considered large if more than half of the LD surface is in contact with the ER membrane. N >110 cells for each condition; $p < 0.0001$, $p < 0.0001$, and $p < 0.01$; Data are represented as mean ±SD.
(C) WT cells high-pressure cryofixed are observed by electron microscopy (EM) with and without OA treatment. Insets show different LDs in each condition. ER is indicated by white arrowheads. Dark dots are ribosomes. Ribosome free zones (yellow stars) are in close contact with LD in OA treatment conditions. Red lines delineate LD surface, blue lines indicate ER bilayer, and blue arrowheads indicate points where the ER seems to unzip around the LD in some focal planes. Scale bars, 500 nm (full view) and 100 nm (inset). Quantification of ER-LD contact is performed on N=120 LDs: on the section planes, the ER-LD contacts are either large, not visible or ambiguous.
(D) Cells are treated with OA and chemically fixed and observed using EM. Examples of section plans where LDs appear to be in contact with the ER lumen (white arrows) are shown. Schematic diagram describing the plausible topology of the EM images. Quantification of ER-LD contact is shown in Figure S4C. Scale bar, 500 nm (full view) and 100 nm (inset).
(E) Example of a section plan where ER membranes are recruited around an LD. The ER bilayer seems to unzip at the edge of the LD (in the inset, the ER membrane is drawn in white and the LD surface in red). Scale bar is 500 nm. Related to Figures S4C and S4D.
See also Figure S4.

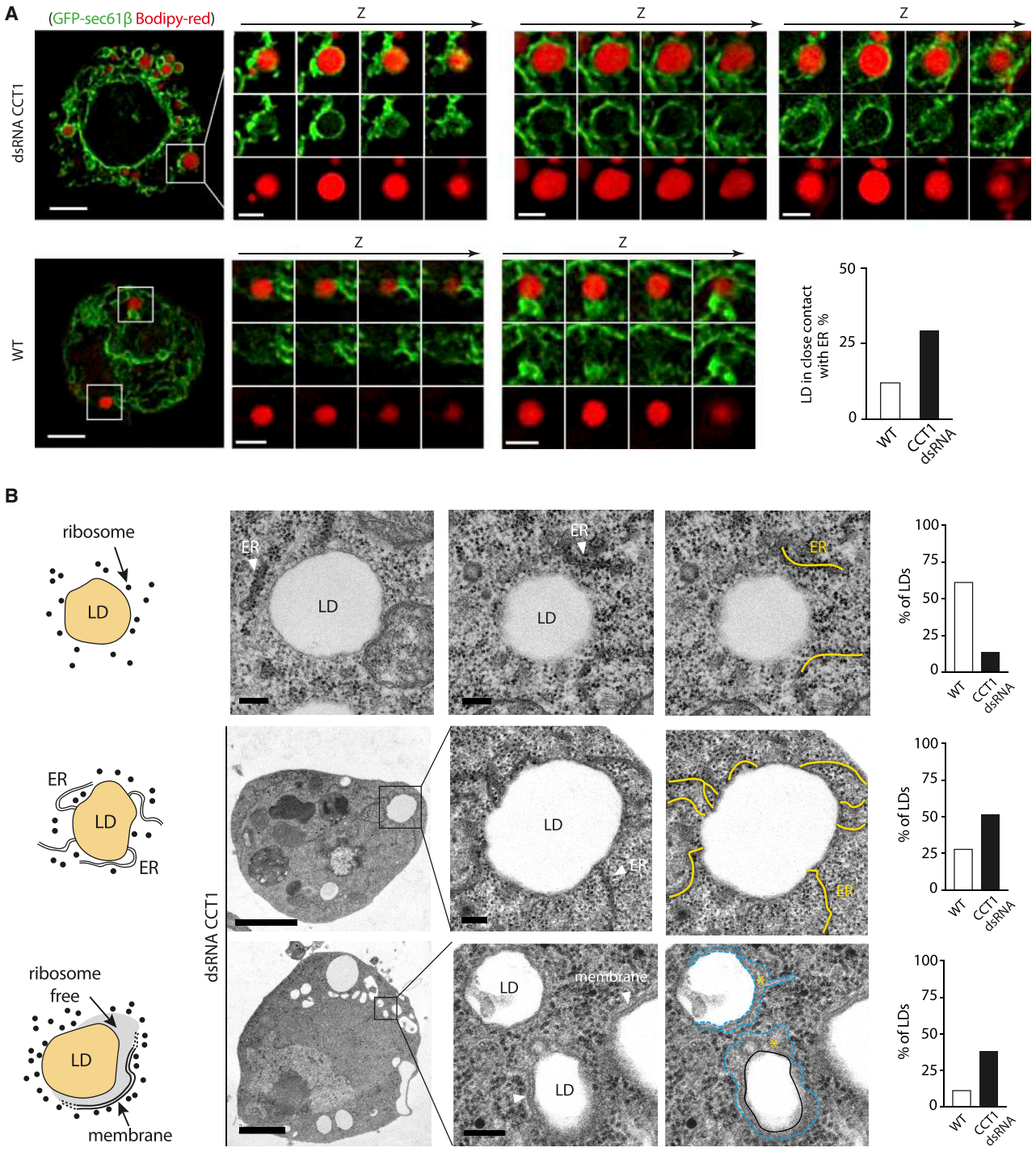

Figure 5. Drosophila Cells with Decreased CCT1 Display Increased ER-LD Contacts

(A) *Drosophila* cells were depleted of CCT1 by dsRNA. LDs are induced by oleate and stained by BODIPY558/568; GFP-sec61β marks the ER. Top: representative confocal image of dsRNA CCT1 cells. Insets show z stacks of LDs in close contact with the ER membrane marker. Bottom left: representative WT control with z stacks of example LDs. The ER-LD contact was less pronounced. Bottom right: dsRNA CCT1 cells present a higher number of LDs in close contact with the ER (quantification made for N =150 in each condition). Scale bar, 2 μm and 200 nm (inset). See Figure S5B for additional z stacks.

(B) WT and CCT1 depleted Drosophila cells treated with OA were fixed by glutaraldehyde and observed by electro-microscopy following contrastation with uranyl acetate and lead. In the section plane, three different LD-ER interactions are defined: top, LDs with no visible contact with ER; middle, LDs with multiple contact point with ER membrane; and bottom, LDs in large contact, with a noticeable ribosome free zone delineated by the ER membrane. Frequency of these phenotypes in WT and dsRNA CCT1 cells is shown on the right with an average of fifteen LDs each. More Illustrative EM images are presented in Figure S5E. Scale bar, 2 μm and 200 nm for zoomed insets. See also Figure S5.

see right examples) and was reminiscent of what an LD-associated protein signal would look like. This observation revealed that these LDs were in close contact with the ER lumen. We next performed EM imaging and found that CCT1 depletion led to significantly more ER-connected LDs (Figure 5B). We also found another significant phenotype where the LDs had regions devoid of ribosomes and delineated by membranes, which were probably the ER. This phenotype is reminiscent of the one observed in yeast (Figure 4C), where LDs are probably in contact with the ER lumen.

Model LDs Equally Emerge on Both Membrane Sides If Phospholipids Are Not Replenished

To further understand the ER-associated LD phenotypes, we opted for the DEV set-up to mimic the absence of a phospholipid refilling mechanism to the cytosolic monolayer, under conditions where many LDs are generated. We made PC DEVs with many small and symmetrically positioned artificial LDs (Figure 6A). Under these conditions, the aLD-to-bilayer surface ratio was ~2% (Figure 6A), close to LD-to-ER surface ratios in yeast (Figure 3D). We then decreased the DEV tension, by deflating them with a hypertonic buffer added to the aqueous medium, to promote spontaneous emergence of the droplets (Deslandes et al., 2017; Chorlay and Thiam, 2018). By following droplets of the same DEV, we observed that they fully emerged, interestingly, into both sides of the bilayer (Figures 6B, 6C, S6A, and S6B). These results were highly reproducible and the budding events into the internal and external sides were statistically equal (Figure 6D).

This even distribution of emerged artificial LDs across the bilayer probably arose from a compensatory mechanism of surface expansion (Figure S6C). The external and internal monolayers of the bilayer had initially approximately the same phospholipid coverage. When an artificial LD emerged, e.g., toward the exterior, it expanded the external leaflet surface area, while the amount of phospholipids remained constant on the time scale of droplet budding (because flip-flop rates are extremely slow for PC (Tieleman and Marrink, 2006; Nakano et al., 2009)). Expansion of the external leaflet reduced this monolayer phospholipid coverage as compared to the internal monolayer; therefore, emergence of the second droplet was favored toward the opposite leaflet (Figure S6C). Emergence of the second droplet re-equilibrate the surface coverage between the two monolayers and so on and so forth. This feedback mechanism can explain the increased number of LDs that stayed in contact with the ER lumen (Figures 4 and 5): in ER membranes unable to provide enough phospholipids to the cytoplasmic monolayer, the emergence of an LD population into the cytosol will tend to expose of the rest of the LDs to the lumen.

To fully prove this emergence feedback mechanism, we made a PC DEV with one large artificial LD (Figure 6E), with a droplet-to-bilayer surface of 22% (Figure 6F), close to the situation where many LDs are formed in yeast cells (Figure 3D). The aLD was symmetrically positioned in the bilayer (Figures 6E and 6G). With a micropipette, we suctioned out a small portion of the droplet and removed it, which mimics emergence from the ER of a given total aLD volume or surface (Figures 6E and S6D). This operation removed phospholipids from the outer monolayer, reducing its coverage as compared to the inner one. As expected, the remaining total aLD volume becomes more exposed toward the side with the better phospholipid coverage, i.e., the luminal side (Figures 6E and 6G). Emergence to the luminal side was evident after slightly decreasing the bilayer tension or internal pressure (previously increased by the ablation step) (Figures 6E, 6G, and 6H); note that simply decreasing this tension or pressure without the induced phospholipid coverage asymmetry was not solely sufficient to induce such emergence (Figure S6H). A cross section of a 3D visualization of the final system demonstrating the internal emergence is shown in Figures 6H and S6F. In conclusion, this experiment is evidence that in the absence of phospholipid replenishment, the budding of a droplet population toward the membrane side will promote the emergence of the rest of the droplets to the opposite side.

Finally, we estimated that the difference in monolayer coverage that induced the aLD internal emergence was about 9%, corresponding to an imbalance of monolayer surface tension of less than 8% (Figures 6I and S6G). Because our experimental condition reproduced LD/ER surface ratios found in yeast cells boosted with LDs, our findings suggest that maintaining an excess of around 9% of phospholipids on the cytosolic monolayers of the ER is sufficient to guarantee proper LD formation in the cytosol during high lipogenesis regimes.

DISCUSSION

In the present work, we show that LDs bud off and emerge toward the membrane side with higher monolayer leaflet coverage. LDs rapidly absorb this asymmetry by emerging on the side of higher coverage. Because *in vivo* LDs mainly emerge to the cytosol, our results suggest that during lipogenesis, the cytosolic monolayer coverage should transiently be kept higher than the luminal monolayer coverage. We shed light on the mechanisms that maintain such tension imbalances.

The strong adsorption of proteins from the cytosol improves the coverage of the monolayer surface by masking possible phospholipid packing defects of the monolayer (Bacle et al., 2017; Prévost et al., 2018; Thiam et al., 2013b). Thereupon, adsorbed proteins lower the surface tension of the cytosolic monolayer and imposes LD emergence in the cytosol (Figure 7A). This directional emergence could be also mediated by ER-embedded proteins that target LDs. Most of these proteins are indeed strongly attached to the LD cytosolic monolayer by using AHs and/or hairpin motifs (Kassan et al., 2013; Pol et al., 2014; Wilfling et al., 2013; Jacquier et al., 2013; Huang and Huang, 2017).

More generally, the strong binding of any protein to the monolayer of a nascent LD will tend to retain the LD into this monolayer compartment (Figure 7B). Thus, proteins that would strongly bind LDs from the cytosol and the ER lumen would compete for LD emergence. Depending on the binding affinity of these proteins, an LD could be trapped in the ER membrane with various degrees of contact with the ER lumen and the cytosol (Figure 7B). This probably explains how in hepatocytes ApoB100 retains some mature LDs in the ER lumen because of its irreversible binding to the LD surface (Figure S1F). In these cells, ApoB binds only to some LDs to possibly make them accessible to ER luminal proteins, which is important for the secretion of very low-density lipoprotein (Ohsaki et al., 2008, 2009). Similarly, LD retention in the ER lumen is also likely caused by the overexpression of Perilipin constructs targeted to the ER

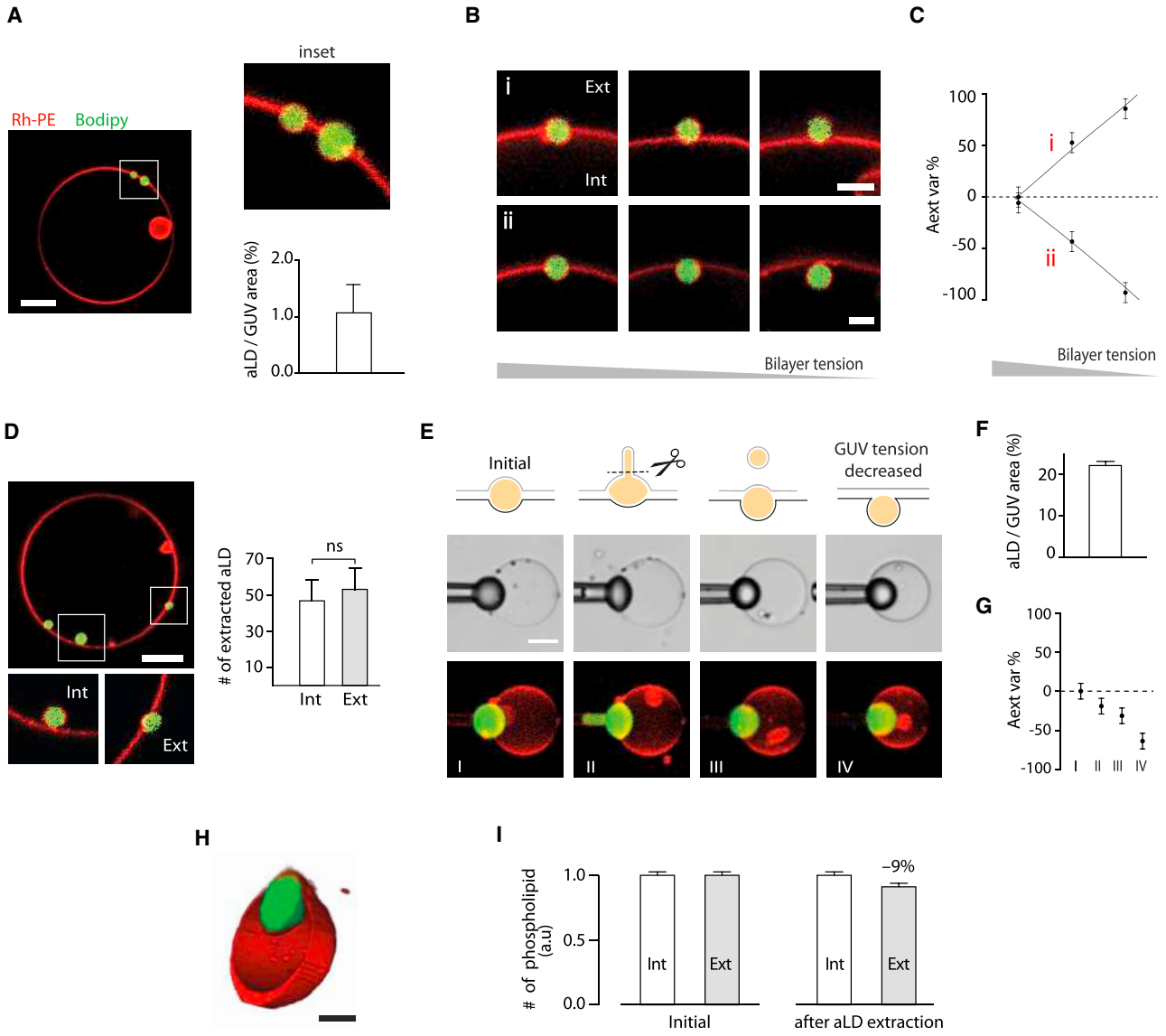

Figure 6. Artificial LDs Equally Emerge on Both Sides of a Same Bilayer with Fixed Phospholipid Number

(A) Example of a confocal image of DEV with small artificial LDs; the DEV contains other aLDs, which were not visible in the shown confocal plane. Bodipy stained the droplet and Rhodamine-PE (Rh-PE) labeled the membranes. The inset is zoomed. The graph shows the quantification of the total artificial LDs surface over the GUV bilayer apparent area (See Figure S6B). Scale bar, 10 μm. Error bar is the measurement precision.

(B) Example of two LDs in the same DEV that emerge on different directions upon decreasing the DEV bilayer tension. Scale Bar, 2.5 μm. An extremely deflated GUV with aLDs emerged on both bilayer side is shown in Figure S6A).

(C) The external area variation ("Aext var") is shown for the two aLDs that emerged on different directions in (B). Error bar is the measurement precision.

(D) Example and quantification of the number of aLDs that emerged in the interior and exterior of DEVs. Scale bar, 10 μm. t test showed ns difference; N = 100. Data are represented as mean ± SD.

(E) Mimic of the budding of a total lipid droplet number (or aLD total surface) from a bilayer. The aLD of a DEV is suctioned on the exterior and ablated (see Figure S6D) to mimic emergence of a certain LD volume, or surface, from the bilayer. The remaining artificial LD is displaced in the bilayer lumen. Deflating the DEV to reduce its surface tension led to almost complete exposing the remained artificial LD into the lumen (full data see Figure S6E). Scale bar, 10 μm.

(F) Quantification of the total aLD surface over the GUV bilayer initial apparent area. Error bar is the measurement precision.

(G) The aLD external area variation corresponding to (E). Error bar is the measurement precision.

(H) 3D reconstitution of the inward emerged aLD (see Figure S6F). Scale bar, 10 μm.

(I) Quantification, based on the ablated aLD surface, of the relative change in the phospholipid number between the internal and external monolayers. Figure S6G shows the related external and internal monolayer tension generated. Error bar is the measurement precision.

See also Figure S6.

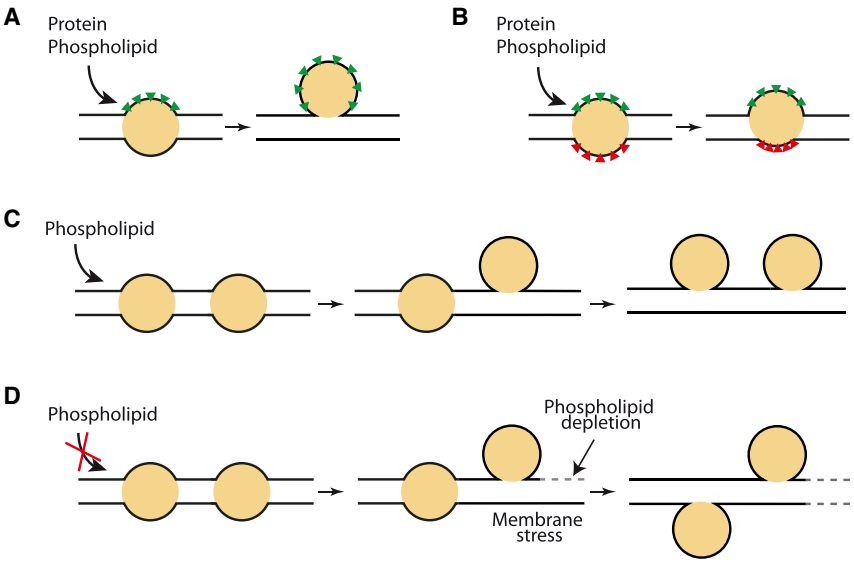

Figure 7. Proposed Model for the Impact of Proteins and Phospholipids on LD Emergence

(A) Recruitment of both proteins and phospholipids to one monolayer promotes LD emergence toward this monolayer side.

(B) A balance of strongly inserted proteins will position an LD in the bilayer with various degree of contact to the surrounding aqueous phases.

(C) Continuous injection of phospholipid on the upper monolayer promotes LD emergence to the upper side.

(D) Lack of a monolayer phospholipid excess, or supply, induces LD equal emergence to both membrane sides, membrane stress, and reorganization.

lumen. Indeed, in such cases LDs become accessible to ER luminal proteins (Mishra et al., 2016). Thus, the overexpression or downregulation of any protein that is able to tightly bind to the LD surface will affect LD emergence (Figure 7B). For LDs to fully emerge into the cytosol, proteins with high affinity for an LD surface should not get access to LD from the ER lumen. One possible way to fence out proteins, especially those coming from the luminal side, is provided by some specific proteins localized to LD biogenesis sites such as Seipin (Wang et al., 2016; Chen and Goodman, 2017; Thiam and Beller, 2017; Grippa et al., 2015).

The release of multiple ER-derived LDs into the cytosol will reduce the number of phospholipids in the ER cytosolic leaflet. Hence, this leaflet needs to be refilled to guarantee that all LDs bud in the same direction while preserving ER morphology (Figure 7C). Otherwise, chances are that LDs get in large contact within the ER lumen (Figure 7D). In *Saccharomyces cerevisiae* and *Drosophila* cells deficient in PCT1 and CCT1 enzymes respectively, or in phospholipids, many LDs indeed failed to fully emerge in the cytosol.

Excess phospholipids on the cytosolic monolayer will make the ER asymmetric, at least under lipogenesis conditions during which phospholipid synthesis is triggered on the cytosolic ER leaflet (Lagace and Ridgway, 2013; Walker et al., 2011; Van Meer et al., 2008). Thus, the idea that the ER has a symmetric membrane needs to be reconsidered. During lipogenesis conditions, the ER may actually display regions where an asymmetry in phospholipid type and density is generated for controlling the LD emergence side. For example, early lipidomic studies of ER-derived microsomes from rat liver have shown that the ER outer leaflet is more enriched in PC and less in phosphatidylethanolamine (Higgins and Dawson, 1977). Also, phospholipids are provided in an asymmetric fashion by the fusion with the ER of retrograde transport vesicles. These vesicles are derived from the Golgi that is asymmetrical in lipid composition (Van Meer et al., 2008) and have more and different phospholipids on their outer monolayer. Finally, the exclusive phosphate phosphatase activity of FIT2 in the ER luminal membrane side suggests at least a transient asymmetry of the membrane in phosphatidic acid.

Regarding the asymmetry in phospholipid density, various mechanisms can enable the refill of the cytosolic leaflet with phospholipids. *De novo* phospholipid biosynthesis is probably the primary mechanism fulfilling such need (Lagace and Ridgway, 2013; Van Meer et al., 2008). Enzymes of the Kennedy pathway for *de novo* PC biosynthesis are indeed important for LD emergence (Lagace and Ridgway, 2013; Krahmer et al., 2011; Aitchison et al., 2015) (Figures 5 and S4A). Alternatively, ER-embedded flippases (Bishop and Bell, 1985) might transfer phospholipids from the ER luminal to the cytosolic monolayer to control LD emergence. The unselective insertion of proteins into the ER cytosolic monolayer may also increase the phospholipid density in this monolayer (Segrest et al., 2015). Finally, FIT2 is also a potential factor promoting ER membrane asymmetry in phospholipid density. By its presumable phosphate phosphatase activity in the ER luminal monolayer (Becuwe et al., 2018; Hayes et al., 2017), FIT2 may convert phospholipids of this monolayer into diacylglycerols. These molecules are soluble in the neutral lipid phases and will be released from the luminal monolayer into the lipid phase; next, they could be reconverted into phospholipids on the cytosolic monolayer. Hence, FIT2 activity would result in a net phospholipid transfer from the ER luminal leaflet to the cytosolic one. Such action would maintain LD emergence toward the cytosol.

Finally, membrane curvature may also help LD emergence (Figures 2I–2K). However, the emergence of LDs in the cytosol will deplete the cytosolic monolayer of phospholipids, unless these are refilled. This would introduce an asymmetry in monolayer phospholipid coverage that would favor inward emergence. These antagonist effects would perturb the tubular membrane topology and later formed LDs would remain in contact with the ER lumen. This situation will induce phenotypes where growing LDs, which are more exposed to the lumen, become tightly opposed to the ER membrane. Hence, the often-reported ER-wrapped phenotype may be a signature of a defect in LD emergence.

In conclusion, our findings bring insights on mechanisms of cytosolic LD biogenesis and their link with ER morphology and phospholipid biosynthesis. Our data support the hypothesis that the ER membrane undergoes dynamic asymmetrical remodeling during lipogenesis periods, so as to guarantee LD

formation in the cytosol, which is critical for the LD proteome and subsequent biological functions.

STAR★METHODS

Detailed methods are provided in the online version of this paper and include the following:

- KEY RESOURCES TABLE
- CONTACT FOR REAGENT AND RESOURCE SHARING
- EXPERIMENTAL MODEL AND SUBJECT DETAILS
  - Yeast Strain and Culture Media Conditions
  - Huh7.5 Culture and Media Conditions
  - *Drosophila* Kc167 Culture Media Conditions
- METHOD DETAILS
  - DEV Preparation: GUVs + LDs
  - Determination of the Degree of LD Emergence in the DEV Experimental System
  - Determination of the Coverage Asymmetry
  - Determination of the Shape and Position of an LD in a GUV Bilayer
  - Proteins Production and Purification
  - Protein Enrichment of the DEV External Leaflet
  - Micromanipulation & Surface Tension Measurements by Micro Aspiration
  - Pendent Droplet Interfacial Tension Measurements
  - Triolein-Protein Surface Tension Measurement
  - Triolein-Phospholipid Surface Tension Measurement
  - Lyso-PC Enrichment to the GUV External Leaflet
  - Molecular Dynamics (MD) Simulations
  - Time Scale of LD Emergence and Phospholipid Flipping
  - Lipid Droplet Induction and Fluorescence Microscopy of Yeast Cells
  - Electron Microscopy Experiments in Yeast Cells
  - Thin Layer Chromatography and Lipid Detection
  - dsRNAs Construction for Drosophila Experiments
  - Structured Illumination Microscopy of Drosophila Experiments
  - qPCR Confirmation of CCT1 Knock-Down in Drosophila Experiments
  - Electron Microscopy Experiments of Drosophila Cells
  - Modulation of GUVs Bilayer Tension Using Osmotic Pressure
  - Calculation of the Amount of Removed Phospholipids
- QUANTIFICATION AND STATISTICAL ANALYSIS
  - Quantification Methods in Yeast
  - Quantification in Drosophila cells
  - Statistical Analysis
- DATA AND SOFTWARE AVAILABILITY

SUPPLEMENTAL INFORMATION

Supplemental Information can be found online at https://doi.org/10.1016/j.devcel.2019.05.003.

ACKNOWLEDGMENTS

We are thankful to Dr. David Savage and Bruno Antonny for the kind gift of proteins, Alisa Gahlen and Elisabeth John for technical support, and Astrid Schauss and Felix Babatz from the CECAD Imaging Facility for EM imaging. We thank all the group members for their valuable comments and critical discussions. This work was supported the ANR-NanoDrop to A.R.T. and L.M., ANR-LDEN, ANR-Mobil, ANR-18-CE11-0012-01, and Paris Sciences et Lettres to A.R.T.

AUTHOR CONTRIBUTIONS

A.C. and A.R.T. designed the research and experiments and quantified all data. A.C. performed all *in vitro* experiments, with the help of K.B.M. and M.O., and D.A. performed the lipid analysis. S.W., J.F., E.J., and P.C. performed the yeast and the electron microscopy experiments. M.B. did the studies in *Drosophila* cells, and L.M. performed the molecular dynamics studies. R.B. purified proteins and helped on the elaboration of *in vitro* experiments. A.R.T. wrote the manuscript and all the authors reviewed and edited it.

DECLARATION OF INTERESTS

The authors declare no competing interests.

Received: April 26, 2018
Revised: January 11, 2019
Accepted: May 2, 2019
Published: May 30, 2019

REFERENCES

Aitchison, A.J., Arsenault, D.J., and Ridgway, N.D. (2015). Nuclear-localized CTP:phosphocholine cytidylyltransferase alpha regulates phosphatidylcholine synthesis required for lipid droplet biogenesis. Mol. Biol. Cell *26*, 2927–2938.

Ajjaji, D., Mbarek, K.B., Mimmack, M.L., England, C., Herscovitz, H., Dong, L., Kay, R.G., Patel, S., Saudek, V., Small, D.M., et al. (2019). Dual binding motifs underpin the hierarchical association of perilipins1-3 with lipid droplets. Mol. Biol. Cell *30*, 703–716.

Antonny, B., Beraud-Dufour, S., Chardin, P., and Chabre, M. (1997). N-terminal hydrophobic residues of the G-protein ADP-ribosylation factor-1 insert into membrane phospholipids upon GDP to GTP exchange. Biochemistry *36*, 4675–4684.

Bacle, A., Gautier, R., Jackson, C.L., Fuchs, P.F.J., and Vanni, S. (2017). Interdigitation between triglycerides and lipids modulates surface properties of lipid droplets. Biophys. J. *112*, 1417–1430.

Beck, R., Sun, Z., Adolf, F., Rutz, C., Bassler, J., Wild, K., Sinning, I., Hurt, E., Brügger, B., Béthune, J., et al. (2008). Membrane curvature induced by Arf1-GTP is essential for vesicle formation. Proc. Natl. Acad. Sci. USA *105*, 11731–11736.

Becuwe, M., Bond, L.M., Mejhert, N., Boland, S., Elliott, S.D., Cicconet, M., Liu, X.N., Graham, M.M., Walther, T.C., and Farese, R.V. (2018). FIT2 is a lipid phosphate phosphatase crucial for endoplasmic reticulum homeostasis. bioRxiv.

Ben M'barek, K., Ajjaji, D., Chorlay, A., Vanni, S., Forêt, L., and Thiam, A.R. (2017). ER membrane phospholipids and surface tension control cellular lipid droplet formation. Dev. Cell *41*, 591–604.e7.

Bigay, J., Gounon, P., Robineau, S., and Antonny, B. (2003). Lipid packing sensed by ArfGAP1 couples COPI coat disassembly to membrane bilayer curvature. Nature *426*, 563–566.

Bishop, W.R., and Bell, R.M. (1985). Assembly of the endoplasmic reticulum phospholipid bilayer: the phosphatidylcholine transporter. Cell *42*, 51–60.

Brasaemle, D.L. (2007). Thematic review series: adipocyte biology. The perilipin family of structural lipid droplet proteins: stabilization of lipid droplets and control of lipolysis. J. Lipid Res. *48*, 2547–2559.

Carman, G.M., and Henry, S.A. (1989). Phospholipid biosynthesis in yeast. Annu. Rev. Biochem. *58*, 635–669.

Chen, X., and Goodman, J.M. (2017). The collaborative work of droplet assembly. Biochim. Biophys. Acta Mol. Cell Biol. Lipids *1862*, 1205–1211.

Chorlay, A., and Thiam, A.R. (2018). An asymmetry in monolayer tension regulates lipid droplet budding direction. Biophys. J. *114*, 631–640.

Choudhary, V., Golani, G., Joshi, A.S., Cottier, S., Schneiter, R., Prinz, W.A., and Kozlov, M.M. (2018). Architecture of lipid droplets in endoplasmic reticulum is determined by phospholipid intrinsic curvature. Curr. Biol. *28*, 915–926.e9.

Choudhary, V., Ojha, N., Golden, A., and Prinz, W.A. (2015). A conserved family of proteins facilitates nascent lipid droplet budding from the ER. J. Cell Biol. *211*, 261–271.

Cole, N.B., Murphy, D.D., Grider, T., Rueter, S., Brasaemle, D., and Nussbaum, R.L. (2002). Lipid droplet binding and oligomerization properties of the Parkinson's disease protein alpha-synuclein. J. Biol. Chem. *277*, 6344–6352.

Copic, A., Antoine-Bally, S., Gimenez-Andres, M., La Torre Garay, C., Antonny, B., Manni, M., Pagnotta, S., Guihot, J., and Jackson, C. (2018). A giant amphipathic helix from a perilipin that is adapted for coating lipid droplets. Nature Communications *9*, https://doi.org/10.1038/s41467-018-03717-8.

Deslandes, F., Thiam, A.R., and Forêt, L. (2017). Lipid droplets can spontaneously bud off from a symmetric bilayer. Biophys. J. *113*, 15–18.

Dowd, S.R., Bier, M.E., and Patton-Vogt, J.L. (2001). Turnover of phosphatidylcholine in Saccharomyces cerevisiae. J. Biol. Chem. *276*, 3756–3763.

Farge, E., and Devaux, P.F. (1992). Shape changes of giant liposomes induced by an asymmetric transmembrane distribution of phospholipids. Biophys. J. *61*, 347–357.

Fujimoto, T., and Parton, R.G. (2011). Not just fat: the structure and function of the lipid droplet. Cold Spring Harb. Perspect. Biol. *3*, a004838.

Gaspar, M.L., Aregullin, M.A., Jesch, S.A., and Henry, S.A. (2006). Inositol induces a profound alteration in the pattern and rate of synthesis and turnover of membrane lipids in Saccharomyces cerevisiae. J. Biol. Chem. *281*, 22773–22785.

Griesbauer, J., Wixforth, A., and Schneider, M.F. (2009). Wave propagation in lipid monolayers. Biophys. J. *97*, 2710–2716.

Grillitsch, K., Connerth, M., Köfeler, H., Arrey, T.N., Rietschel, B., Wagner, B., Karas, M., and Daum, G. (2011). Lipid particles/droplets of the yeast Saccharomyces cerevisiae revisited: lipidome meets proteome. Biochim. Biophys. Acta *1811*, 1165–1176.

Grippa, A., Buxó, L., Mora, G., Funaya, C., Idrissi, F.Z., Mancuso, F., Gomez, R., Muntanyà, J., Sabidó, E., and Carvalho, P. (2015). The seipin complex Fld1/Ldb16 stabilizes ER-lipid droplet contact sites. J. Cell Biol. *211*, 829–844.

Guo, Y., Walther, T.C., Rao, M., Stuurman, N., Goshima, G., Terayama, K., Wong, J.S., Vale, R.D., Walter, P., and Farese, R.V. (2008). Functional genomic screen reveals genes involved in lipid-droplet formation and utilization. Nature *453*, 657–661.

Hayes, M.J., Choudhary, V., Ojha, N., Shin, J.J., Han, G.S., Carman, G.M., Loewen, C.J., Prinz, W.A., and Levine, T.P. (2017). Fat storage-inducing transmembrane (FIT or FITM) proteins are related to lipid phosphatase/phosphotransferase enzymes. Microb. Cell *5*, 88–103.

Henne, W.M., Reese, M.L., and Goodman, J.M. (2018). The assembly of lipid droplets and their roles in challenged cells. EMBO J. *37*.

Higgins, J.A., and Dawson, R.M.C. (1977). Asymmetry of the phospholipid bilayer of rat liver endoplasmic reticulum. Biochim. Biophys. Acta *470*, 342–356.

Huang, C.Y., and Huang, A.H.C. (2017). Unique motifs and length of hairpin in oleosin target the cytosolic side of endoplasmic reticulum and budding lipid droplet. Plant Physiol. *174*, 2248–2260.

Jacquier, N., Choudhary, V., Mari, M., Toulmay, A., Reggiori, F., and Schneiter, R. (2011). Lipid droplets are functionally connected to the endoplasmic reticulum in Saccharomyces cerevisiae. J. Cell Sci. *124*, 2424–2437.

Jacquier, N., Mishra, S., Choudhary, V., and Schneiter, R. (2013). Expression of oleosin and perilipins in yeast promotes formation of lipid droplets from the endoplasmic reticulum. J. Cell Sci. *126*, 5198–5209.

Kassan, A., Herms, A., Fernández-Vidal, A., Bosch, M., Schieber, N.L., Reddy, B.J., Fajardo, A., Gelabert-Baldrich, M., Tebar, F., Enrich, C., et al. (2013). Acyl-CoA synthetase 3 promotes lipid droplet biogenesis in ER microdomains. J. Cell Biol. *203*, 985–1001.

Khandelia, H., Duelund, L., Pakkanen, K.I., and Ipsen, J.H. (2010). Triglyceride blisters in lipid bilayers: implications for lipid droplet biogenesis and the mobile lipid signal in cancer cell membranes. PLoS One *5*, e12811.

Krahmer, N., Guo, Y., Wilfling, F., Hilger, M., Lingrell, S., Heger, K., Newman, H.W., Schmidt-Supprian, M., Vance, D.E., Mann, M., et al. (2011). Phosphatidylcholine synthesis for lipid droplet expansion is mediated by localized activation of CTP:phosphocholine cytidylyltransferase. Cell Metab. *14*, 504–515.

Lagace, T.A., and Ridgway, N.D. (2013). The role of phospholipids in the biological activity and structure of the endoplasmic reticulum. Biochim. Biophys. Acta *1833*, 2499–2510.

Laouini, A., Jaafar-Maalej, C., Limayem-Blouza, I., Sfar, S., Charcosset, C., and Fessi, H. (2012). Preparation, characterization and applications of liposomes: state of the art. J. Colloid Sci. Biotechnol. *1*, 147–168.

Londos, C., Brasaemle, D.L., Gruia-Gray, J., Servetnick, D.A., Schultz, C.J., Levin, D.M., and Kimmel, A.R. (1995). Perilipin: unique proteins associated with intracellular neutral lipid droplets in adipocytes and steroidogenic cells. Biochem. Soc. Trans. *23*, 611–615.

Martin, S., and Parton, R.G. (2006). Lipid droplets: a unified view of a dynamic organelle. Nat. Rev. Mol. Cell Biol. *7*, 373–378.

Mishra, S., Khaddaj, R., Cottier, S., Stradalova, V., Jacob, C., and Schneiter, R. (2016). Mature lipid droplets are accessible to ER luminal proteins. J. Cell Sci. *129*, 3803–3815.

Murphy, D.J., and Vance, J. (1999). Mechanisms of lipid-body formation. Trends Biochem. Sci. *24*, 109–115.

Nakano, M., Fukuda, M., Kudo, T., Matsuzaki, N., Azuma, T., Sekine, K., Endo, H., and Handa, T. (2009). Flip-flop of phospholipids in vesicles: kinetic analysis with time-resolved small-angle neutron scattering. J. Phys. Chem. B *113*, 6745–6748.

Ohsaki, Y., Cheng, J., Suzuki, M., Fujita, A., and Fujimoto, T. (2008). Lipid droplets are arrested in the ER membrane by tight binding of lipidated apolipoprotein B-100. J. Cell Sci. *121*, 2415–2422.

Ohsaki, Y., Cheng, J., Suzuki, M., Shinohara, Y., Fujita, A., and Fujimoto, T. (2009). Biogenesis of cytoplasmic lipid droplets: from the lipid ester globule in the membrane to the visible structure. Biochim. Biophys. Acta *1791*, 399–407.

Olzmann, J.A., and Carvalho, P. (2019). Dynamics and functions of lipid droplets. Nat. Rev. Mol. Cell Biol. *20*, 137–155.

Ostermeyer, A.G., Paci, J.M., Zeng, Y., Lublin, D.M., Munro, S., and Brown, D.A. (2001). Accumulation of caveolin in the endoplasmic reticulum redirects the protein to lipid storage droplets. J. Cell Biol. *152*, 1071–1078.

Pol, A., Gross, S.P., and Parton, R.G. (2014). Review: biogenesis of the multifunctional lipid droplet: lipids, proteins, and sites. J. Cell Biol. *204*, 635–646.

Pomorski, T., and Menon, A.K. (2006). Lipid flippases and their biological functions. Cell. Mol. Life Sci. *63*, 2908–2921.

Pomorski, T.G., and Menon, A.K. (2016). Lipid somersaults: uncovering the mechanisms of protein-mediated lipid flipping. Prog. Lipid Res. *64*, 69–84.

Prévost, C., Sharp, M.E., Kory, N., Lin, Q., Voth, G.A., Farese, R.V., and Walther, T.C. (2018). Mechanism and determinants of amphipathic helix-containing protein targeting to lipid droplets. Dev. Cell *44*, 73–86.e4.

Rajan, A., and Perrimon, N. (2012). Drosophila cytokine unpaired 2 regulates physiological homeostasis by remotely controlling insulin secretion. Cell. *151*, 123–137.

Rowe, E.R., Mimmack, M.L., Barbosa, A.D., Haider, A., Isaac, I., Ouberai, M.M., Thiam, A.R., Patel, S., Saudek, V., Siniossoglou, S., et al. (2016). Conserved amphipathic helices mediate lipid droplet targeting of perilipins 1-3. J. Biol. Chem. *291*, 6664–6678.

Salo, V.T., Belevich, I., Li, S., Karhinen, L., Vihinen, H., Vigouroux, C., Magré, J., Thiele, C., Hölttä-Vuori, M., Jokitalo, E., and Ikonen, E. (2016). Seipin regulates ER-lipid droplet contacts and cargo delivery. EMBO J. *35*, 2699–2716.

Schwarz, D.S., and Blower, M.D. (2016). The endoplasmic reticulum: structure, function and response to cellular signaling. Cell. Mol. Life Sci. *73*, 79–94.

Segrest, J.P., Jones, M.K., Catte, A., Manchekar, M., Datta, G., Zhang, L., Zhang, R., Li, L., Patterson, J.C., Palgunachari, M.N., et al. (2015). Surface density-induced pleating of a lipid monolayer drives nascent high-density lipoprotein assembly. Structure *23*, 1214–1226.

Sui, X., Arlt, H., Brock, K.P., Lai, Z.W., Dimaio, F., Marks, D.S., Liao, M., Farese, R.V., and Walther, T.C. (2018). Cryo-electron microscopy structure of the lipid droplet-formation protein seipin. J. Cell Biol. *217*, 4080–4091.

Thiam, A.R., Antonny, B., Wang, J., Delacotte, J., Wilfling, F., Walther, T.C., Beck, R., Rothman, J.E., and Pincet, F. (2013a). COPI buds 60-nm lipid droplets from reconstituted water-phospholipid-triacylglyceride interfaces, suggesting a tension clamp function. Proc. Natl. Acad. Sci. USA *110*, 13244–13249.

Thiam, A.R., and Beller, M. (2017). The why, when and how of lipid droplet diversity. J. Cell Sci. *130*, 315–324.

Thiam, A.R., Farese, R.V., Jr., and Walther, T.C. (2013b). The biophysics and cell biology of lipid droplets. Nat. Rev. Mol. Cell Biol. *14*, 775–786.

Thiam, A.R., and Forêt, L. (2016). The physics of lipid droplet nucleation, growth and budding. Biochim. Biophys. Acta *1861*, 715–722.

Thiam, A.R., and Pincet, F. (2015). The energy of COPI for budding membranes. PLOS ONE *10*, e0133757.

Tieleman, D.P., and Marrink, S.J. (2006). Lipids out of equilibrium: energetics of desorption and pore mediated flip-flop. J. Am. Chem. Soc. *128*, 12462–12467.

Van Meer, G., Voelker, D.R., and Feigenson, G.W. (2008). Membrane lipids: where they are and how they behave. Nat. Rev. Mol. Cell Biol. *9*, 112–124.

Vevea, J.D., Garcia, E.J., Chan, R.B., Zhou, B.W., Schultz, M., Di Paolo, G., Mccaffery, J.M., and Pon, L.A. (2015). Role for lipid droplet biogenesis and microlipophagy in adaptation to lipid imbalance in yeast. Dev. Cell *35*, 584–599.

Walker, A.K., Jacobs, R.L., Watts, J.L., Rottiers, V., Jiang, K., Finnegan, D.M., Shioda, T., Hansen, M., Yang, F., Niebergall, L.J., et al. (2011). A conserved SREBP-1/phosphatidylcholine feedback circuit regulates lipogenesis in metazoans. Cell *147*, 840–852.

Wang, H., Becuwe, M., Housden, B.E., Chitraju, C., Porras, A.J., Graham, M.M., Liu, X.N., Thiam, A.R., Savage, D.B., Agarwal, A.K., et al. (2016). Seipin is required for converting nascent to mature lipid droplets. Elife *5*, e16582.

Wang, S., Idrissi, F.Z., Hermansson, M., Grippa, A., Ejsing, C.S., and Carvalho, P. (2018). Seipin and the membrane-shaping protein Pex30 cooperate in organelle budding from the endoplasmic reticulum. Nat. Commun. *9*, 2939.

Wei, D., Jacobs, S., Modla, S., Zhang, S., Young, C.L., Cirino, R., Caplan, J., and Czymmek, K. (2012). High-resolution three-dimensional reconstruction of a whole yeast cell using focused-ion beam scanning electron microscopy. BioTechniques *53*, 41–48.

Welte, M.A. (2015). Expanding roles for lipid droplets. Curr. Biol. *25*, R470–R481.

West, M., Zurek, N., Hoenger, A., and Voeltz, G.K. (2011). A 3D analysis of yeast ER structure reveals how ER domains are organized by membrane curvature. J. Cell Biol. *193*, 333–346.

Wilfling, F., Thiam, A.R., Olarte, M.-J., Wang, J., Beck, R., Gould, T.J., Allgeyer, E.S., Pincet, F., Bewersdorf, J., and Farese, R.V. (2014). Arf1/COPI machinery acts directly on lipid droplets and enables their connection to the ER for protein targeting. Elife *3*, e01607.

Wilfling, F., Wang, H., Haas, J.T., Krahmer, N., Gould, T.J., Uchida, A., Cheng, J.X., Graham, M., Christiano, R., Fröhlich, F., et al. (2013). Triacylglycerol synthesis enzymes mediate lipid droplet growth by relocalizing from the ER to lipid droplets. Dev. Cell *24*, 384–399.

Yan, R., Qian, H., Lukmantara, I., Gao, M., Du, X., Yan, N., and Yang, H. (2018). Human seipin binds anionic phospholipids. Dev. Cell *47*, 248–256.e4.

Zanghellini, J., Wodlei, F., and von Grünberg, H.H. (2010). Phospholipid demixing and the birth of a lipid droplet. J. Theor. Biol. *264*, 952–961.

Zimmerberg, J., and Kozlov, M.M. (2006). How proteins produce cellular membrane curvature. Nat. Rev. Mol. Cell Biol. *7*, 9–19.

STAR★METHODS

KEY RESOURCES TABLE

REAGENT or RESOURCE	SOURCE	IDENTIFIER
Chemicals, Peptides, and Recombinant Proteins		
Phospholipids (DOPC, Rhodamine-DOPE, LysoPC (18:1))	Avanti Polar Lipids	https://avantilipids.com/
Triolein	Sigma Aldrich	T7140
Bovine Serum Albumin (BSA)	Sigma Aldrich	A7906-100G
Dithionite	Sigma Aldrich	71699-250G
Apolipoprotein B from human plasma	Sigma Aldrich	SRP6302
Plin1 108-137, Purity 96.83% (NBD-PPEKIASELKDTISTRLRSARNSISVPIAS)	ProteoGenix, France	https://www.proteogenix.science/
CAV fragment 159-178, Purity 96.83% (NBD-LFEAVGKIFSNVRINLQKEI)	Peptide 2.0, USA	https://www.peptide2.com/
Alpha-Synuclein	Bruno Antonny's lab, IPMC CNRS	N/A
Plin1 fragment 93-192	Pr. David Savage (Cambridge Metabolic Research Laboratories, UK).	N/A
Fluorescently labeled Arf1	This study, see Method Details	N/A
Monodansyl pentane (MDH)	Abgent	SM1000a
Oleic acid	Sigma Aldrich	O1008-1G
Inositol	Sigma	I5125-50G
Yeast nitrogen base with ammonium sulfate	MP Biomedicals	4027-522
Yeast nitrogen base with ammonium sulfate, without inositol	MP Biomedicals	4027-412
CSM-HIS-LEU-TRP-URA	MP Biomedicals	4550-022
Bacto yeast extract	BD	212750
Bactopeptone	BD	211677-500G
Fluorescently labeled C12 fatty acid	Thermo Fisher / Molecular Probes	D3835
Fatty acid free Bovine Serum Albumin (BSA)	Sigma Aldrich	A8806
Oleic acid	Calbiochem	4954
Experimental Models: Cell Lines		
S. cerevisiae: (BY4741) *MATa ura3Δ0his3Δ1leu2Δ0met15Δ0* SEC63-mNeonGreen-HIS	This paper	yPC10613
S. cerevisiae: (BY4741) *MATa ura3Δ0his3Δ1leu2Δ0met15Δ0pct1::KAN* SEC63-mNeonGreen-HIS	This paper	yPC10672
Human hepatocytes Huh7.5	Apath Missouri	APC 49
Drosophila Kc167	Harvard RNAi screening center	https://fgr.hms.harvard.edu
Oligonucleotides		
CCT1_RNAi_fwd: gtaatacgactcactataggATCGGAAGTTCAGGATCAGC	Harvard RNAi Screening Center	DRSC08157
CCT1_RNAi_rev: gtaatacgactcactataggCCCGCTGAAGAATTGCTG	Harvard RNAi Screening Center	DRSC08157
CCT1_RNAi_fwd: gtaatacgactcactataggGATGGCCACCTCATCGATAC	Harvard RNAi Screening Center	DRSC27869
CCT1_RNAi_rev: gtaatacgactcactataggCTTTGTGAGATGGTGCGTGT	Harvard RNAi Screening Center	DRSC27869
rp49_fwd: ATCGGTTACGGATCGAACAA	(Rajan et al., 2012)	N/A
rp49_rev: GACAATCTCCTTGCGCTTCT	(Rajan et al., 2012)	N/A

(*Continued on next page*)

Continued

REAGENT or RESOURCE	SOURCE	IDENTIFIER
CCT1_qPCR_fwd: GGAAGCGGACCTACGAGATA	(Copic et al., 2018)	N/A
CCT1_qPCR_rev: GTGCCCTGATCCTGAACTT	(Copic et al., 2018)	N/A
Recombinant DNA		
pA-GFP-W-sec61ß	Tobias Walther's laboratory, Harvard Medical School	N/A
Software and Algorithms		
Matlab R2016a	Licence of the École Normale Supérieure	https://fr.mathworks.com
Fiji	Online	https://imagej.net/Fiji
Adobe illustrator CS4	Licence of the École Normale Supérieure	N/A
GraphPad Prism 7.0a	Licence of the École Normale Supérieure	https://graphpad.com/scientific-software/prism/
GROMACS v5.1.4	Online	http://www.gromacs.org/

CONTACT FOR REAGENT AND RESOURCE SHARING

Further information and requests for reagents may be directed to and will be fulfilled by the Lead Contact, Abdou Rachid Thiam (thiam@ens.fr).

EXPERIMENTAL MODEL AND SUBJECT DETAILS

Yeast Strain and Culture Media Conditions

Saccharomyces cerevisiae cell strains used in the experiments are yPC10613 (*MATa ura3Δ0his3Δ1leu2Δ0met15Δ0* SEC63-mNeonGreen-HIS) and yPC10672 (*MATa ura3Δ0his3Δ1leu2Δ0met15Δ0pct1::KAN* SEC63-mNeonGreen-HIS). Cells were grown at 30°C in YPD liquid medium (1% yeast extract, 2% peptone, 2% glucose).

Huh7.5 Culture and Media Conditions

Huh7.5 were maintained in Dulbecco's modified Eagle's medium (DMEM) supplemented with 10% heat inactivated fetal bovine serum (Life Technologies), 0.1 gL-1 sodium pyruvate (Life Technologies) and 1% penicillin-streptomycin (Life Technologies). The cells were cultured at 37°C under a 5% CO2 atmosphere.

Drosophila Kc167 Culture Media Conditions

Drosophila Kc167 cells were grown in Schneider's Drosophila medium with L-Glutamine including 10% heat inactivated fetal calf serum (medium and serum from PAN Biotech, Aidenbach, Germany) with Penicillin/Streptomycin.

METHOD DETAILS

DEV Preparation: GUVs + LDs

Unless mentioned, *in vitro* experiments were performed in the following HKM buffer: 50 mM Hepes, 120 mM Kacetate, and 1 mM MgCl2 (in Milli-Q water) at pH 7.4 and 275±15 mOsm.

All GUVs were 99.5 % DOPC 0.5% (w/w) Rhodamine-DOPE. GUVs were prepared by electro-formation (Thiam et al., 2013a). Phospholipids and mixtures thereof in chloroform at 0.5 μM were dried on an indium tin oxide (ITO) coated glass plate. The lipid film was desiccated for 1 h. The chamber was sealed with another ITO coated glass plate. The lipids were then rehydrated with a sucrose solution (275+-15 mOsm). Electro-formation is performed using 100 Hz AC voltage at 1.0 to 1.4 Vpp and maintained for at least 1 h. This low voltage was used to avoid hydrolysis of water and dissolution of the titanium ions on the glass plate. GUVs were either stored in the chamber at 4°C overnight or directly collected with a Pasteur pipette.

To prepare the artificial lipid droplets (aLDs), 5 μL of the oil was added to 45 μL of HKM buffer. The mixture was sonicated. The diameter of the resulting droplets is on the order of a few hundred nanometers. To make DEV, GUVs were then incubated with the LDs for 5 min. The GUV-LD mixture was then placed on a glass coverslip pretreated with 10 % (w/w) BSA and washed three times with buffer.

Determination of the Degree of LD Emergence in the DEV Experimental System

We characterized the degree of emergence of the aLD from the bilayer by comparing the inner and outer surface areas of the droplets (Figure 1C). This was assessed by considering the inner and outer surfaces of the LD as spherical caps. All micrographs of *in vitro* systems were made on a Carl ZEISS LSM 800. Glass coverslips: Menzel Glaser (24x36mm #0).

Determination of the Coverage Asymmetry

The asymmetry in the monolayer coverage, is directly related to the surface tension asymmetry which is reflected by the angles formed by the droplet with the bilayer (α and θ, see Figure 1C). More precisely we defined ''coverage asymmetry'' parameter as $(\alpha - \theta)/180$.

If the two LD monolayers present the same coverage, i.e. the same surface tension, α and θ are equal, and ''coverage asymmetry'' parameter is 0. When the external coverage is increased, i.e. external surface tension decreases, α increases, and θ diminishes (Chorlay and Thiam, 2018, STAR Methods: Determination of the shape and position of an LD in a GUV bilayer). This results in an increasing of the ''coverage asymmetry'' parameter. In the limit of a drastic improvement of the external monolayer coverage, provoking a full emergence of the LD, θ is equal to zero, α to 180 degrees and the ''coverage asymmetry'' parameter is equal to 1. O the opposite configuration, i.e. strong improvement of the external monolayer coverage, If the LD would emerge in the opposite direction, and the ''coverage asymmetry'' parameter would the be -1.

Determination of the Shape and Position of an LD in a GUV Bilayer

(adapted from Chorlay and Thiam Biophysical Journal 2018)

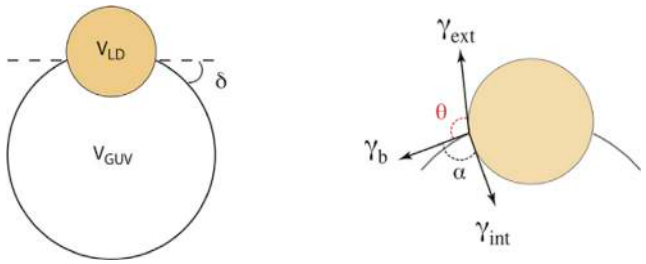

Considering that the aLD's shape is driven by the equilibrium of the three surface tensions (bilayer γ_b, external monolayer γ_{ext} and internal monolayer γ_{int}) (Equation 1), can be projected on the bilayer axis and lead to (Equation 2).

$$\overrightarrow{\gamma_b} + \overrightarrow{\gamma_{int}} + \overrightarrow{\gamma_{ext}} = \overrightarrow{0} \quad \text{(Equation 1)}$$

$$\gamma_b = -\gamma_{int}\cos(\alpha) - \gamma_{ext}\cos(\theta) \quad \text{(Equation 2)}$$

$$\gamma_{ext}\sin(\theta) = \gamma_{int}\sin(\alpha)$$

Moreover, the conserved volume of the LD and the GUV gives two other equations (Equations 3 and 4):

$$V_{LD} = \frac{4\,\Pi Ro^3}{3}\left(\frac{2-\cos(\theta-\delta)^3+3\cos(\theta-\delta)}{\sin(\theta-\delta)^3}+\frac{2-\cos(\alpha-\delta)^3+3\cos(\alpha-\delta)}{\sin(\alpha-\delta)^3}\right) \quad \text{(Equation 3)}$$

$$V_{GUV} = \frac{4\,\Pi Ro^3}{3}\left(\frac{2-\cos(\delta)^3+3\cos(\delta)}{\sin(\delta)^3}-\frac{2-\cos(\alpha-\delta)^3+3\cos(\alpha-\delta)}{\sin(\alpha-\delta)^3}\right) \quad \text{(Equation 4)}$$

In order to determine the shape of the droplet, we only need three parameters: alpha, theta and delta, as a function of the tensions γ_b, γ_{int} and γ_{ext}.

Rearranging these equations leads to a set of 3 equations (Equations 5, 6, and 7) that can be solved numerically.

The following equations (Equations 5 and 6) Gives alpha and theta:

$$\cos(\theta) = \frac{\gamma_{int}^2 - \gamma_{ext}^2 - \gamma_b^2}{2\,\gamma_b\,\gamma_{ext}} \quad \text{(Equation 5)}$$

$$\cos(\alpha) = \frac{\gamma_{ext}^2 - \gamma_{int}^2 - \gamma_b^2}{2\,\gamma_b\,\gamma_{int}} \quad \text{(Equation 6)}$$

The last parameter delta is determined numerically, keeping the volumes constant (Equation 7):

$$\frac{V_{LD}}{V_{GUV}} = \frac{\frac{2-\cos(\theta-\delta)^3+3\cos(\theta-\delta)}{\sin(\theta-\delta)^3} + \frac{2-\cos(\alpha-\delta)^3+3\cos(\alpha-\delta)}{\sin(\alpha-\delta)^3}}{\frac{2-\cos(\delta)^3+3\cos(\delta)}{\sin(\delta)^3} - \frac{2-\cos(\alpha-\delta)^3+3\cos(\alpha-\delta)}{\sin(\alpha-\delta)^3}} \quad \text{(Equation 7)}$$

The simulation displayed in Figures 2I and 2J are obtain using this mathematical model and varying the Vld/Vguv parameter.

Proteins Production and Purification

Cytosol extract was obtained from hepatocyte Huh7.5 cells: confluent monolayers of Huh7.5 cells were placed on ice, washed twice with ice-cold PBS at pH 7.4, and then incubated with 10 mM Tris/HCl, pH 7.4 buffer for 5 minutes on ice. The cells were scraped into a homogenization buffer comprising 10 mM Tris/HCl, 1 mM EGTA, 0.5 mM EDTA and 0.25 M sucrose, pH 7.4, which also contained Complete TM protease inhibitors. The cells were homogenized by twenty in/out passages within a syringe fin needle. The homogenate was transferred to ultracentrifugation tube (2 ml) and were centrifuged for 1 h at 100 000 G at 4°C. The resulting supernatant was used as a cytosol extract.

Fluorescently labeled Arf1 was generated using an Arf1-variant in which the single cysteine residue of Arf1 was replaced with serine, and the C-terminal lysine was replaced with cysteine, yielding Arf1- C159S-K181C. Published work has demonstrated that exchanging the C-terminal lysine of the small GTPase with a Cys- residue, and subsequent fluorescent labeling (using thiol-reactive dyes on Cys181), does not inhibit Arf1-function (Beck et al., 2008). In short, human Arf1- C159S-K181C and yeast N-myristoyltransferase were coexpressed in Escherichia coli supplied with BSA-loaded myristate. Cell lysates were subjected to 35% ammonium sulfate, and the precipitate, enriched in myristoylated Arf1, was further purified by DEAE-ion exchange. Eluted fractions of interest were concentrated in spin-column filters with a 10-kD cutoff (Millipore), and fluorescently labeled using Cy3-maleimide (GE Healtcare) according to the manufacturer's protocol. To remove excess dye, samples were purified by gel filtration using a Superdex 75 column (GE Healthcare).

Protein Enrichment of the DEV External Leaflet

A DEV hold by a glass micropipette is observed by confocal microscopy. 5 μL of protein solution is injected in the 100 μL bulk phase of the DEV solution. The resulting effective concentrations were respectively: Arf1 (1μM); CAV159-178 (5μM); Alpha-Synuclein (5.5μM); ApolipoproteinB (0.1 μM); Plin1 fragment 93-192 (4.7μM); BSA (75μM); The DEV is then followed for ~ 40 min. Solutions were injected at similar spots from the pipette.

Micromanipulation & Surface Tension Measurements by Micro Aspiration

Micro-pipettes were made from capillaries drawn out with a Sutter Instruments pipette-puller. They were used to manipulate the LD-embedded GUVs in order to get a side view of the system. The pipettes were incubated for 30 min in a 5% bovine serum albumin solution (BSA) before use, in order to prevent droplets and membranes from adhering to the glass.

Additionally, surface tensions were measured and modulated using the same pipettes. As shown in (Figure 1I), the micromanipulation of the external LD monolayer enables the measurement of the eternal monolayer surface tension. Using Laplace's law, and the measurement of the pipette inner diameter, droplet diameter, and suction pressure, the surface tension of the interface can be determined:

$$\gamma = \frac{\Delta Psuc}{2\left(\frac{1}{Rp} - \frac{1}{Rd}\right)},$$

where ΔPsuc, Rp and Rd are the suction pressure, the pipette radius and the droplet external radius.

The suction was carried out using a syringe. The resulting pressure was measured with a pressure transducer (DP103 provided by Validyne Eng. Corp, USA), the output voltage of which was monitored with a digital voltmeter. The pressure transducer (range 55 kPa) was calibrated prior to the experiments. Micro-pipettes made from capillaries (1.0oDx0.58iDx150Lmm 30-0017 GC100-15b Harvard Apparatus) with micropipette puller (Sutter instrument model P-2000). Micromanipulation (Eppendorf TransferMan® 4r). Pressure measurement unit (DP103 provided by Validyne eng. corp, USA).

Pendent Droplet Interfacial Tension Measurements

A pendent droplet tensiometer designed by Teclis Instruments (Longessaigne, France) was used to measure the interfacial tension of oil/water interfaces. All experiments were conducted at room temperature. To create triolein/buffer interfaces, triolein drops (from 5 to 16.0μL) were formed at the tip of a J-needle submerged in 5 mL of HKM buffer.

Triolein-Protein Surface Tension Measurement

5 μl of the solution containing the proteins is added to the bulk buffer while the tension of a triolein/buffer interface is measured. The resulting concentrations of proteins were: Alphaalpha-Synuclein (0.1μM); BSA (1.5μM); ApolipoproteinB (2nM); Plin1 108-137 (1μM);

Plin1 fragment 93-192 (0.09μM). When tension stabilizes, the interface is compressed. The tension at maximum coverage was determined when wrinkles appeared on the surface of the droplet. If no wrinkles were observed, the compression was stopped, the max packing tension was determined after waiting for the relaxation and re-stabilization of the tension.

Triolein-Phospholipid Surface Tension Measurement

To create phospholipid monolayers at the interface, phospholipids were dissolved in the triolein (0.01% w/w). After forming a droplet, the PLs relocate at the interface. The Droplet is then compressed until a tension plateau is reached. This plateau of tension is the tension corresponding to the maximum PL coverage, and evoked as the minimal tension reachable.

Lyso-PC Enrichment to the GUV External Leaflet

A micellar solution of lyso-PC (18:1) in HKM at 10x the CMC is prepared by desiccating the phospholipids dissolved in chloroform and rehydrating them in HKM buffer. In order to get a fluorescent signal, 1% (w/w) of NBD-PE is added to the lyso-PC. The resulting solution is then vortexed and sonicated for 5 min, three times. 5 to 20 μL of this micellar solution is then directly added to the 100 μL GUVs solution already placed under the microscope. This system is then observed with and without LDs embedded in the GUVs.

Molecular Dynamics (MD) Simulations

We built lipid bilayer systems consisting of dioleoylphosphatidylcholine (DOPC) containing triolein (TO) lenses starting from a homogeneous distribution of TO in a DOPC bilayer. All systems featured the same number of TO molecules (7500) and a variable number of DOPC lipids, starting from a symmetric system with 9072 DOPC molecules per monolayer and reducing progressively the number of DOPC molecules in one leaflet, in steps of 100 lipids, to reach a maximum imbalance of 1000 lipids (11% imbalance). For each system, we carried out molecular dynamics (MD) simulations of at least 2 μs, and used the final snapshot as a starting point to build the subsequent stage. The reference symmetric system (9072 lipids in each bilayer) was simulated for 30 μs, and the final system with 11% imbalance was simulated for 10 μs. All systems were simulated at the coarse-grained level, using the MARTINI force field (v2.0, lipid version 2015-06 except for triolein, optimized specifically for the present work).

All simulations were carried out with GROMACS v5.1.4, using a leap-frog stochastic dynamics integrator (sd option in GROMACS), with a time step of 20 fs. Non-bonded interactions were calculated with a cutoff of 1.1 nm, using a Verlet neighborlist scheme (Verlet buffer tolerance of 10^{-6} kJ mol^{-1} ps^{-1} per atom); electrostatic interactions were calculated with a dielectric constant of 15 and shifted from 0 nm, Lennard-Jones were shifted from 0.9 nm. All simulations were run at constant temperature (300 K) and pressure using semi-isotropic pressure coupling (Parrinello-Rahman barostat, time constant of 20 ps, 1 bar in xy and z dimensions), resulting in overall zero surface tension in the system.

Time Scale of LD Emergence and Phospholipid Flipping

In a bilayer containing a lipid droplet, any asymmetry in monolayer coverage is spontaneously absorbed (below a second) by the repositioning of the LD in the bilayer (i.e. its emergence). Indeed, micro-manipulation experiments showed that it is a mechanical equilibrium that is reached quicker than we can see ($\Delta t < 40$ms, from our imaging frame rate) (Chorlay and Thiam, 2018).

An asymmetry can be generating in ER by inserting phospholipids on the outer leaflet. This excess of phospholipids has thus to be detected by a LD for emerging. To assess the time scale of this event, let's consider a 1 m long ER and a speed of propagation of the lateral pressure (i.e. phospholipid density) on a monolayer of 1 m/s, despite it has been estimated around 100 m/s (Griesbauer et al., 2009). In this setting, a LD will sense a fabricated PL in few 10 ms. Consequently the increase of the lateral pressure induced by this new phospholipid will be instantaneously detected by the droplet, which will therefore emerge on this side of higher lateral pressure.

Based on these above points, the time frame to rectify a bilayer asymmetry by the re-positioning of a lipid droplet is in the tenth ms range. This time is much smaller than the flip-flop time of a phospholipid in a bilayer which is in the order of minutes as reported in vitro and in vivo (Pomorski and Menon, 2006), which could rectify the asymmetry.

Altogether, if an asymmetry is created between a bilayer leaflets, a lipid droplet will almost instantaneously expend toward the denser monolayer side and absorb the asymmetry. The more asymmetry created the more the droplet will bulge toward the monolayer with excess phospholipids. The flipping of phospholipids will not be fast enough to rectify the asymmetry between the leaflets.

Lipid Droplet Induction and Fluorescence Microscopy of Yeast Cells

Yeast cells grown as described in the EXPERIMENTAL MODEL AND SUBJECT DETAILS section. For LD induction, cells were grown to exponential growth phase, pelleted, and resuspended in YPD + 0.1% oleic acid (Sigma, #O1008) where indicated. In inositol supplementated experiments, cells were grown in synthetic media lacking inositol, in presence (0.1%) or absence of oleate. After 18h growth, cells were harvested by centrifugation and each culture was resuspended and diluted in the same media in presence of absence of 75μM of inositol.

Cells were imaged at 0h, 6h and 24h upon inositol addition. Similar timepoints were collected for lipid analysis. Fluorescence microscopy was performed at room temperature using the Zeiss Cell Observer HS equipped with a CMOS camera (Hamamatsu ORCA-Flash4.0), controlled by 3i Slidebook6.0 software. A Plan-APOCHROMAT 100x 1.4 objective was used. mNeonGreen and MDH signals were detected using the GFP and DAPI filters respectively, at 600ms exposure.

Electron Microscopy Experiments in Yeast Cells

Yeast cells grown as described above were subjected to high pressure freezing and processed as described in (Wang et al., 2018). Alternatively, 10 ODs of exponentially growing cells were subjected to chemical fixation in 1% glutaraldehyde, 0.2% PFA in 40mM potassium phosphate pH 7 for 12-16h at 4C. Fixed cells were further processed as described in (Choudhary et al., 2015). All grids were imaged in a FEI Tecnai 12 TEM operated at 120 kV using a Gatan OneView digital camera.

Thin Layer Chromatography and Lipid Detection

Lipids were extracted and separated on silica TLC plates (Merck) either in chloroform/methanol/acetone/acetic acid/water (100:20:40:20:10) for phospholipids or in petroleum ether/diethyl ether/acetic acid (90:10:1) for neutral lipids, and detected by iodine vapor staining. Bands were identified by comparison with standards. The quantification of the bands were done using Fiji.

dsRNAs Construction for Drosophila Experiments

dsRNAs targeting CCT1 were prepared according to standard procedures (e.g. Beller et al. PLoS 2008). In brief, we amplified targeting sequences pre-computed from the Drosophila RNAi screening center (www.flyrnai.org) from genomic DNA using oligonucleotides fused to a T7 RNA polymerase promotor (lower case in the oligonucleotide sequences). For CCT1 we used the oligonucleotides corresponding to DRSC08157: fwd: gtaatacgactcactataggATCGGAAGTTCAGGATCAGC, rev: gtaatacgactcactataggCCCGCTGA AGAATTGCTG, or DRSC27869: fwd: gtaatacgactcactataggGATGGCCACCTCATCGATAC, rev: gtaatacgactcactataggCTTTGT GAGATGGTGCGTGT

Following PCR amplification we performed an *in vitro* transcription reaction with the TranscriptAid T7 High Yield Transcription Kit (Thermo Fisher Scientific) or the HiScribe T7 High Yield RNA Synthesis Kit (New England Bioloabs) and purified the dsRNA molecules using the Qiagen RNeasy Mini Kit according to the manufacturer's instructions. The dsRNA was stored at -80°C until use.

Structured Illumination Microscopy of Drosophila Experiments

For the targeting experiment analyzed by structured illumination microscopy we seeded 1 mL of 2.5 x 10[5] cells/mL Drosophila Kc167 cells in wells of 12-well tissue culture plates (Sarstedt, Numbrecht, Germany). Cells were imaged using a Zeiss Elyra structured illumination microscope and a Plan-Apochromat 63x/1.4 oil objective with Z-stacks. Cells were grown in Schneider's Drosophila medium with L-Glutamine including 10% heat inactivated fetal calf serum (medium and serum from PAN Biotech, Aidenbach, Germany) with Penicillin/Streptomycin. Following a 6 to 8 hours recovery phase we transfected the cells with 500 ng of the GFP-tagged Sec61beta expression construct (expression is driven by an actin promotor; kind gift from Tobias Walther) and 500 ng of the respective dsRNA or a water only control using the Effectene transfection reagent from Qiagen (Hilden, Germany) according to the manufacturer's instructions. After three days the cells were serum starved overnight (serum free medium with 0.2% fatty acid free bovine serum albumin) to deplete the cells of already existing LDs. On the next day, the cells were resuspended and transferred to high precision cover slips and allowed to adhere for one hour. Subsequently, the medium was replaced with medium containing 600 μM oleic acid containing 1 μg/mL BODIPY558/568 labeled C12 fatty acids (Thermo/Molecular probes) and incubated for six hours. Subsequently the cells were fixed with 4% paraformaldehyde and embedded in Mowiol containing antifades.

qPCR Confirmation of CCT1 Knock-Down in Drosophila Experiments

We isolated RNA from the frozen cells using the rNeasy Mini Kit (Qiagen). qPCR was performed according to standard procedures with oligos for rp49 (fwd: ATCGGTTACGGATCGAACAA, rev: GACAATCTCCTTGCGCTTCT) and CCT1 (fwd: GGAAGCGGACCTAC GAGATA and rev: GTGCCCTGATCCTGAACTT).

Electron Microscopy Experiments of Drosophila Cells

We added 30 μg of dsRNA or water only as a control to 6-well plates. Subsequently, we added 1 mL of 2 x 10[5] cells/mL Drosophila Kc167 cells in serum free Schneider's Drosophila medium. After 45 min incubation, we added 3 mL of complete Schneider's medium and incubated for four days to allow for knock-down of the target by RNA interference. Subsequently, we added 600 μM OA to the cells and incubated for six hours. Cells from one well per sample were washed with PBS and frozen at -80°C to allow later RNA extraction for qPCR analysis. Cells from a second well of each sample were washed with 0.1 M phosphate buffer and afterwards fixed with 2.5 % glutaraldehyde in 0.1 M phosphate buffer for 30 min. After another wash with 0.1 M phosphate buffer and the cells were mixed with 3 % low melting agar in PBS. Agar was cut into small 1 mm square blocks, washed three times with 0.1 M sodium cacodylate buffer before incubation in 1 % osmium, 10 mg/mL potassium ferrocyanide in 0.1 M sodium cacodylate buffer, followed by three more washed in the cacodylate buffer and an ethanol dehydration series. After 100 % ethanol was added, there were two more washes with epon:ethanol (1:1) and epon:ethanol (3:1), respectively. Subsequently, the blocks were incubated with fresh epon at 4°C over night, and two more hours at room temperature, followed by curing at 60°C for 48 to 72 hours. Ultrathin sections (70 μm) were cut from the blocks using an ultramicrotome (Leica, UC7) and stained with 1.5% uranyl acetate for 20 min and Reynolds lead citrate solution for 3 min. Electron micrographs were recorded with a JEM-2100 Plus Transmission Electron Microscope (JEOL) operating at 80 kV with a Camera OneView 4k 32 bit (Gatan) and the software DigitalMicrograph (Gatan).

Modulation of GUVs Bilayer Tension Using Osmotic Pressure

GUV membranes are water-permeable, thus an osmolarity difference between the lumen and the exterior of the GUV results in a deflation or swelling of the GUV. This increases or decreases the bilayer tension. It is then possible to increase the bilayer tension osmotically with a hypotonic external buffer (e.g. adding MQ water to the HKM buffer surrounding the GUV; standard procedure is 10 μL of MQ water added to the 100 μL of HKM buffer). The bilayer tension can be decreased using a hypertonic external buffer (5 μL of 1M NaCl solution added to the 100 μL of HKM buffer).

Calculation of the Amount of Removed Phospholipids

When mechanically depleting the external leaflet of the GUV-LD system (see Figure 6E), we remove a portion of the PLs by ablating a part of the external monolayer. Assuming that the repartition of the PLs is homogenous on the leaflets, the number of PLs removed from the external leaflet is proportional to the ablated area of leaflet. Then the percentage of removed PLs can be calculated by: area of the removed tongue over total external leaflet area. The internal leaflet remains intact, so the number of PLs on this leaflet is constant.

QUANTIFICATION AND STATISTICAL ANALYSIS

Quantification Methods in Yeast

Aberrant ER: Yeast cells were enumerated according to their ER morphology using a Z projection of Z-stack images. If the cortical and nuclear ER were clearly defined, the cell was considered regular, if unusual ER membrane signals appeared in the cytoplasm, forming of lumps or threads, the cell was considered as aberrant.

Number of LD in Aberrant /Regular cells: Two sets of cells were selected according to the morphology of their ER (see above). Ambiguous cells were discarded. In these two populations the number of LD was quantified in approximately 40 cells in each subset.

LD in large contact with the ER: the proportion of cells presenting at least one event of LD presenting a close contact with ER (on half of its surface or more) was quantified over the total number of cell.

Quantification in Drosophila cells

LD in close contact with the ER: the number of LD surrounded or more than semi surrounded in the ER is quantified over the total number of LD in the cells.

LD size distribution: After preforming a Z projection with the Z-stack images of the LD and a thresholding, a Matlab program calculated the surface of the individual LDs. The statistics on the LD radius was maid (considering the LD as spherically shaped).

Statistical Analysis

The statistical comparisons where made using a non-parametric t-test (GraphPad Prism 7.0a; *** indicates $p < 0.0001$ ** indicates $p < 0,001$ * indicates $p < 0.01$). Unless mentioned, all values shown in the text and figures are mean ± S.D.

DATA AND SOFTWARE AVAILABILITY

All simulations were carried out with GROMACS v5.1.4.

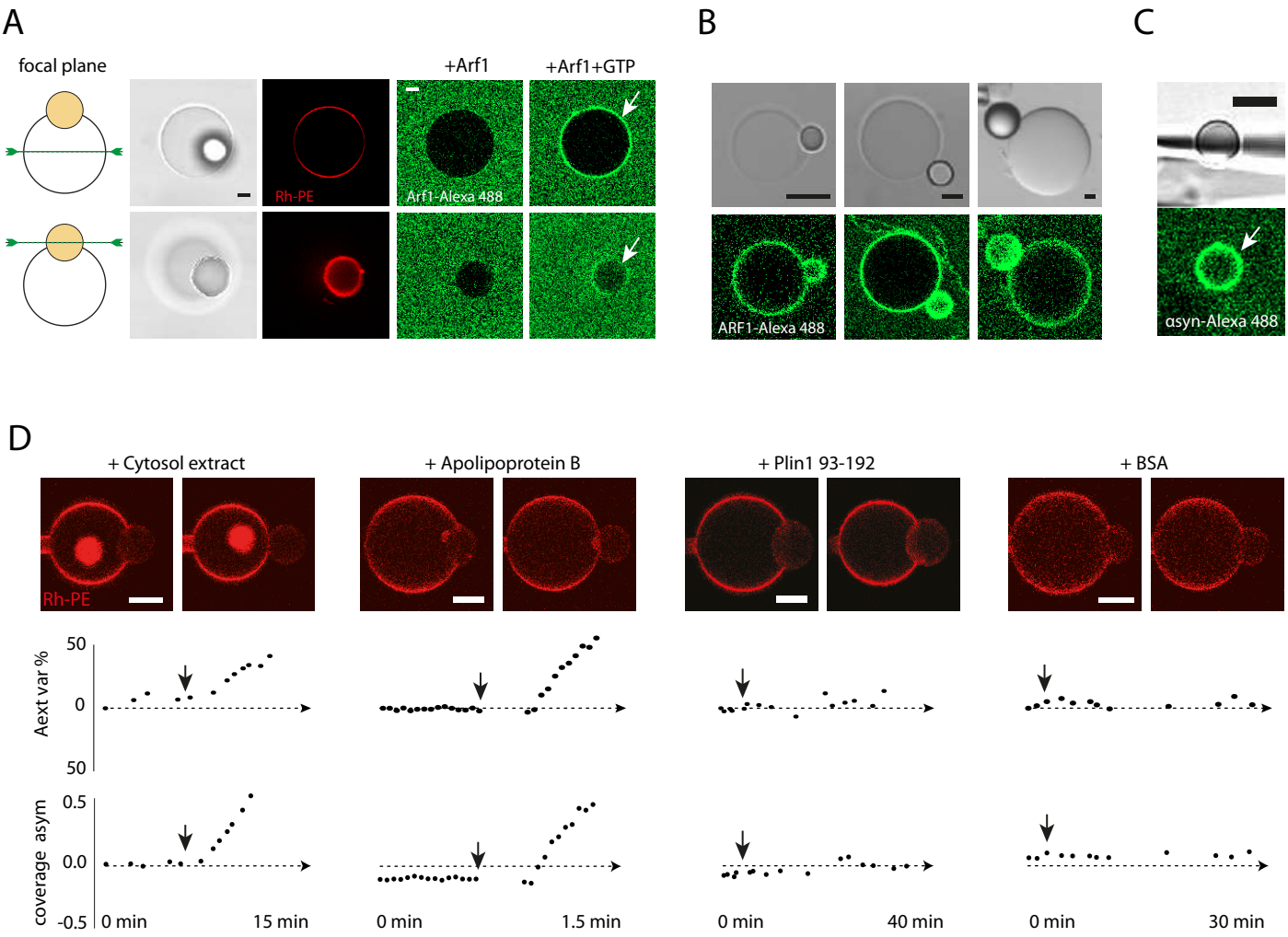

E

Protein fragment	Sequence
Cav 159-178	NBD-L**F**EAVGKI**F**SNVRINLQKEI
Plin1 108 -137	NBD-PPEKIASELKDTISTRLRSARNSISVPIAS
Plin1 93 -192	RGLDHLEEKIPALQ**Y**PPEKIASELKDTISTRLRSARNSISVPIASTSDKVLGAALAGCELA**W**GV ARDTAE**F**AANTRAGRLASGGADLALGSIEKVVE**Y**LL
α-Synuclein	Alexa488-MDV**F**MKGLSKAKEGVVAAAEKTKQGVAEAAGKTKEGVL**Y**VGSKTKEGVVHGVATVAEKTK EQVTNVGGAVVTGVTAVAQKTVEGAGSIAAATG**F**VKKDQLGKNEEGAPQEGILEDMPVDP DNEA**Y**EMPSEEG**Y**QD**Y**EPEA

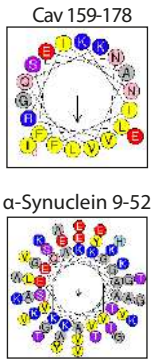

F

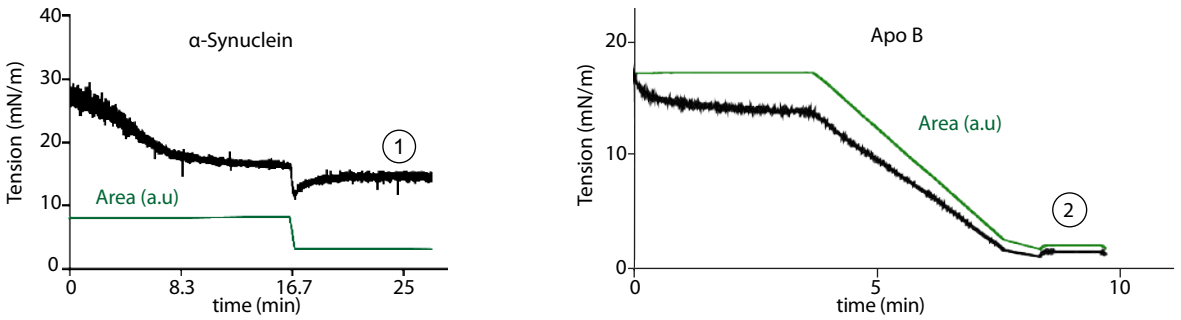

Supplementary Figure S1 | Membrane binding characteristics of the different proteins assessed for LD emergence capacity, related to Figure 1

A) PC DEV with a triolein droplet stained with Rhodamine-PE. Arf1-Alexa488 added to the external medium. Arf1 recruits on the bilayer and the droplet when GTP is added to the external medium. Arrows point to the GUV and droplet interface. Scale bars is 5 µm.

B) Side views of PC DEV with a triolein droplet after incubation with Arf1-Alexa488 + GTP for 20 min. Droplets emerged towards the exterior. Scale bars are 5 µm.

C) Bare triolein droplet after 20 min incubation with Alpha-Synuclein-Alexa488. Alpha-Synuclein-Alexa488 is recruited on the droplet surface. Scale bars is 5 µm.

D) Fluorescence Confocal images of condition displayed in Figure 1G. Red is phospholipids marked with Rhodamine-PE. Scale bars are 10 µm. For each of these conditions, artificial LD external area variation and coverage asymmetry are displayed over time. Arrows indicate proteins injection time.

E) Left: sequences of the proteins fragments used in the Figure 1 experiment; highly hydrophobic residues are highlighted in bold. Right: examples of helix wheels, Cav 159-178 fragment and Alpha-Synuclein 9-52 helix.

F) Droplet surface tension measurement by a droplet tensiometer method (see star methods). A Pure triolein droplet was formed in a buffer phase. Protein solutions were next added to the bulk buffer phase, which was agitated by using a magnetic bead (Left: Alpha-Synuclein; Right: Apolipoprotein B). After waiting for an equilibrium of tension, the droplet surface is decreased and then kept constant. Two different behavior are observed: 1- tension relaxes (Alpha-Synuclein), suggesting ejection of the protein by lateral compression; 2- tension stays constant (Apolipoprotein B), meaning that the protein is strongly bound to the interface; in the latter case the proteins formed a rigid coat that mechanically retained the interface (images not shown). Thus, binding of Apolipoprotein B can mechanically retain a nascent LD into the protein-containing region. Green curves are the droplet surface area (a.u.).

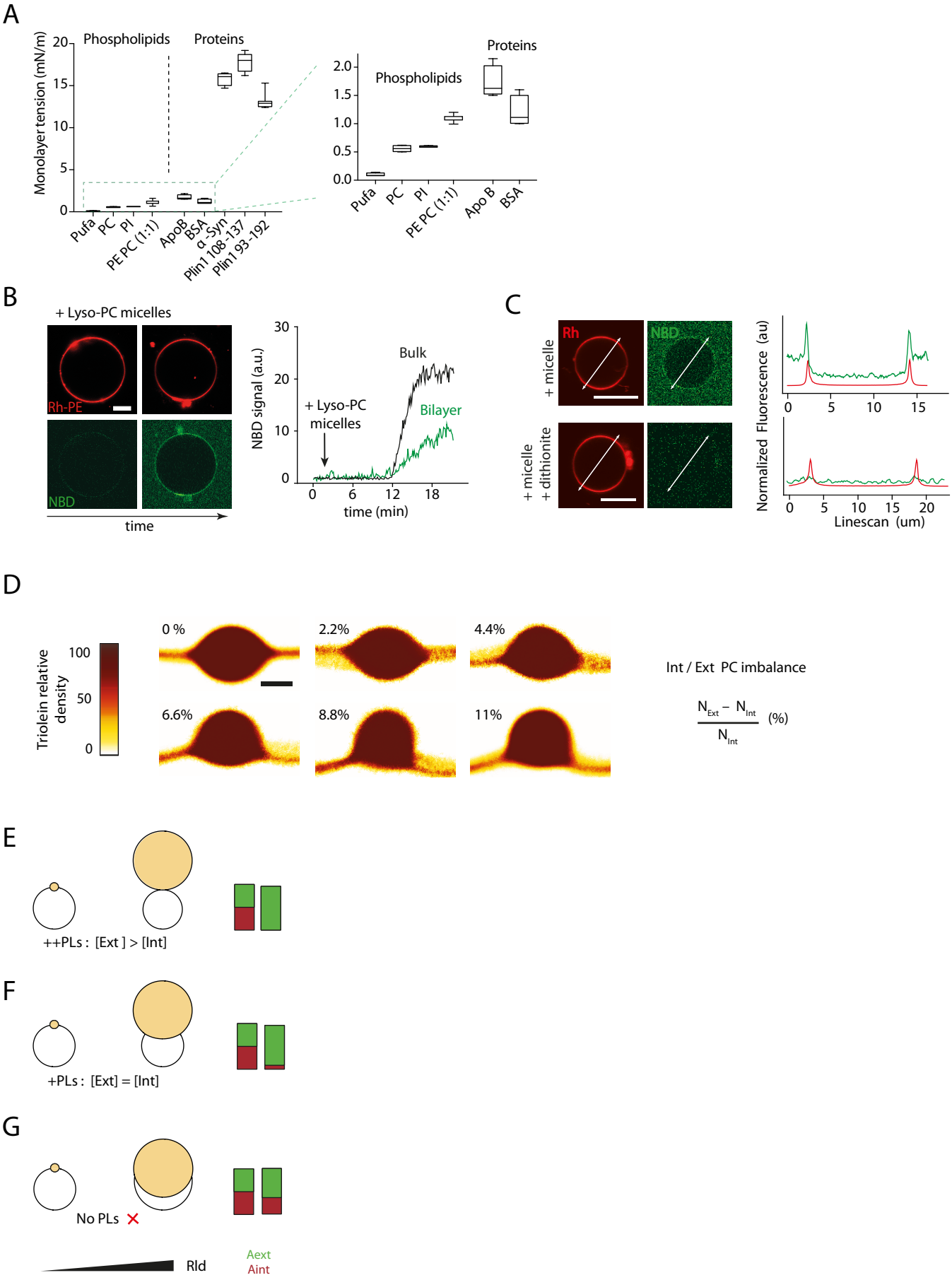
A
Monolayer tension (mN/m)
Phospholipids
Proteins
Pufa
PC
PI
PE PC (1:1)
ApoB
BSA
α-Syn
Plin1 108-137
Plin193-192
Apo B
B
+ Lyso-PC micelles
Rh-PE
NBD
time
NBD signal (a.u.)
Bulk
Bilayer
+ Lyso-PC micelles
time (min)
C
Rh
NBD
+ micelle
+ micelle + dithionite
Normalized Fluorescence (au)
Linescan (um)
D
Triolein relative density
0 %
2.2%
4.4%
6.6%
8.8%
11%
Int / Ext PC imbalance
(%)
E
++PLs : [Ext] > [Int]
F
+PLs : [Ext] = [Int]
G
No PLs
Rld
Aext
Aint

Supplementary Figure S2 | Maintaining an excess of phospholipids and proteins on one monolayer leaflet enables to decrease tension and favors LD full emergence, related to Figure 2

A) Minimal surface tensions of triolein/buffer interface covered by different phospholipids or proteins. These minimal monolayer surface tensions are measured at maximum monolayer packing or pressure, obtained by reducing the volume of the triolein-in-buffer drop (see for example in Figure S1F) (Pufa stands for C18:0 C22:4 polyunsaturated phosphatidylcholine).

B) NBD signal in bulk and on the surface of the GUV over time. After addition, the micellar solution diffuses to reach a GUV. The signal in the GUV vicinity increases which leads to rapid increase of the bilayer signal, meaning lyso-PC recruitment. Scale bar is 10 µm.

C) Linescans through GUVs corresponding to Figure 2B: GUV after Lyso-PC micelles treatment, GUV after Lyso-PC micelles treatment and Dithionite treatment. Red channel: rhodamine-PE marking the GUV membrane, green channel: NBD-PE marking the Lyso-PC micelles. The micelle treatment increases the NBD signal outside of the GUV and fluorescence is recruited on the bilayer. The dithionite treatment quenches all NBD fluorescence. Scale bars are 10 µm.

D) Average density distribution of triolein molecules embedded in the PC bilayer for 0%, 2.2%, 4.4%, 6.6%, 8.8%, 11% PC excess in external leaflet corresponding to Figure 2G,H . Colors heat map give an insight of the probability of triolein molecule presence. Scale bar is 15 nm.

E), Simulated profile showing the plausible behavior of a growing LD where exterior phospholipid coverage is increase during LD growth. This results in a full emergence of the LD.

F), Simulated profile showing the plausible behavior of a growing LD where phospholipids are added to maintain a constant coverage on both monolayers. The LD tends to emerge due to curvature effects. The LD remains always in contact with the interior.

G) Simulated profile showing the plausible behavior of a growing LD. Here no phospholipids are added during growth. Increasing the aLD radius (Rld) expands external monolayer (see Figure 2I,J). This results in a decrease of phospholipid coverage concomitant with an increase of external tension that prevents LD emergence.

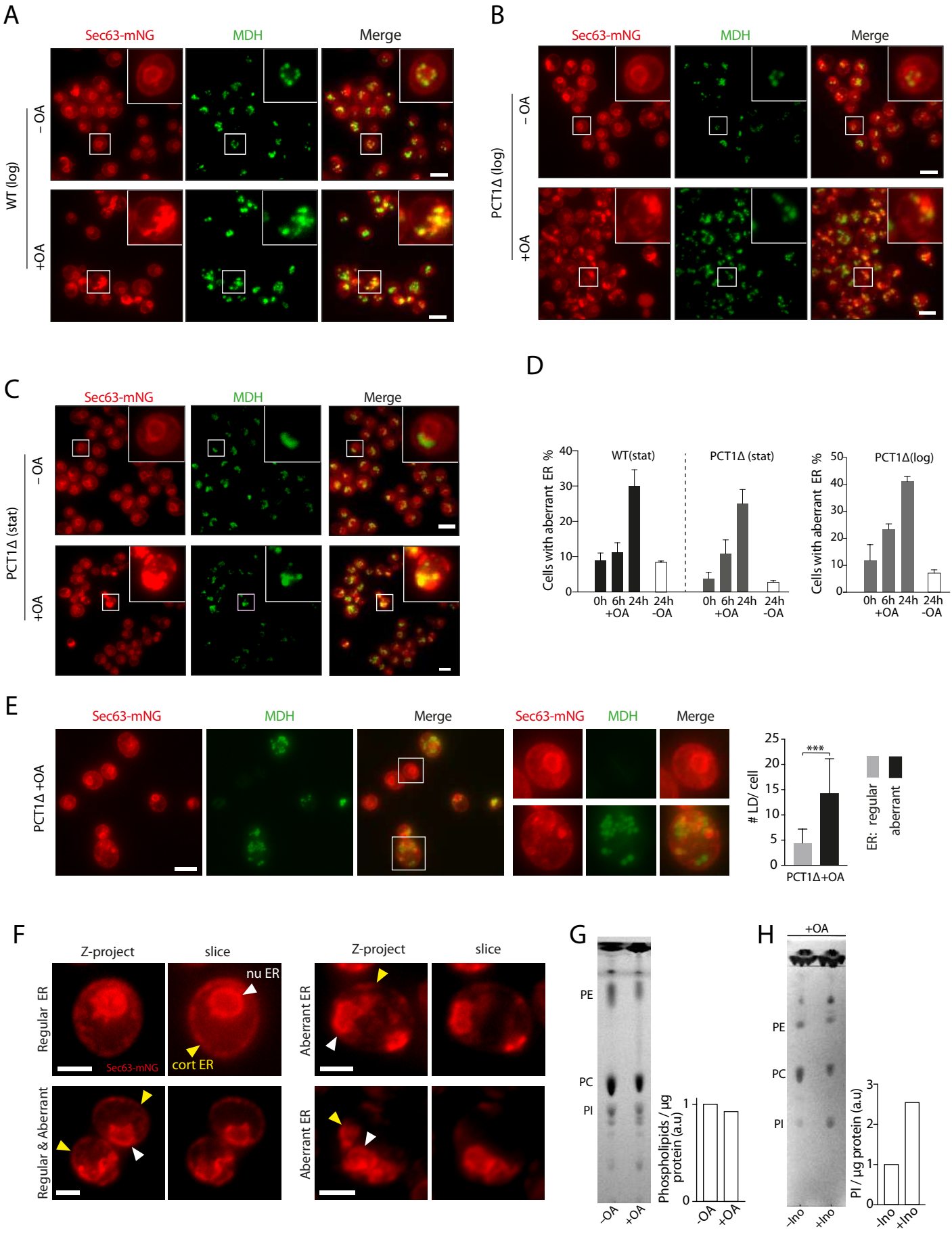
A
Sec63-mNG
MDH
Merge
WT (log)
– OA
+OA
B
PCT1Δ (log)
C
PCT1Δ (stat)
D
Cells with aberrant ER %
WT(stat)
PCT1Δ (stat)
PCT1Δ(log)
0h 6h 24h +OA
24h -OA
E
PCT1Δ +OA
LD/ cell
***
ER: regular
aberrant
F
Z-project
slice
Regular ER
Aberrant ER
Regular & Aberrant
nu ER
cort ER
Sec63-mNG
G
PE
PC
PI
Phospholipids / µg protein (a.u)
-OA
+OA
H
+OA
PI / µg protein (a.u)
-Ino
+Ino

Supplementary Figure S3 | Excess LD formation in *Saccharomyces cerevisiae* cells under logarithmic or exponential phases is associated with ER remodeling, related to Figure 3

A) *Saccharomyces cerevisiae* cells cultured in the presence or not of OA (Oleate) from logarithmic growth phase are imaged at 24 h. The ER marker protein, Sec63, was endogenously tagged with monomeric NeonGreen (Sec63-mNG), and LDs were labeled by monodansylpentane (MDH). Images shown represent z-projection of different planes. Scale bars, 5 μm.

B) PCT1-depleted (*pct1*Δ) *Saccharomyces cerevisiae* cells cultured in the presence or not of OA to logarithmic growth phase are imaged at 24 h. The ER marker protein, Sec63, was endogenously tagged with monomeric NeonGreen (Sec63-mNG), and LDs were labeled by the neutral lipid dye, MDH. Images shown represent z-projection of different planes. Scale bars, 5 μm.

C) PCT1-depleted (*pct1*Δ) *Saccharomyces cerevisiae* cells cultured to stationary phase, imaged after 24 h with or without treatment with oleic acid (OA). Sec63-mNG marked the ER and LDs were stained by MDH. Images shown represent z-projection of different stacks. Scale bars, 5 μm.

D) Corresponding quantification of the number of cells with aberrant ER, 0 h, 6 h and 24 h after OA treatment. Control cells with no OA addition are shown at 24 h time point. N=1300 cells for both *pct1*Δ and WT. Data are represented as mean ±SD.

E) Left: PCT1-deleted *Saccharomyces cerevisiae* cells cultured to stationary phase, after 24h treated with oleic acid (OA). Sec63-mNG marks ER and LD are MDH labeled. Scale bars, 5 μm. Right: Aberrant-ER cells statistically contained more LDs than cells with normal ER. t-test ($p<0.0001$), N = 140 cells, Data are represented as mean ±SD.

F) *Saccharomyces cerevisiae* cells cultured to stationary phase with OA. Phenotypes of regular and aberrant ER are shown displaying Z projection and slice image. ER is Sec63-mNG marked. Yellow arrowheads indicate Cortical ER, white arrowheads indicate nuclear ER. Scale bar are 2 μm.

G) Thin layer chromatography (TLC) experiment: Total amount of Phospholipids/μg of proteins in *Saccharomyces cerevisiae* treated with or without OA. Quantification is shown on the right. Protein concentration in lysate: –OA:2,9μg/mL; +OA: 2,8μg/mL.

H), Thin layer chromatography (TLC) experiment performed with cellular extract of WT cells cultured to stationary phase, after 24h in presence of OA and with or without inositol treatment. Protein concentration in lysate: –inositol: 2,7μg/mL; +Inositiol: 2,4μg/mL. Quantification of PI (Phosphatidylinositol) is shown on the right.

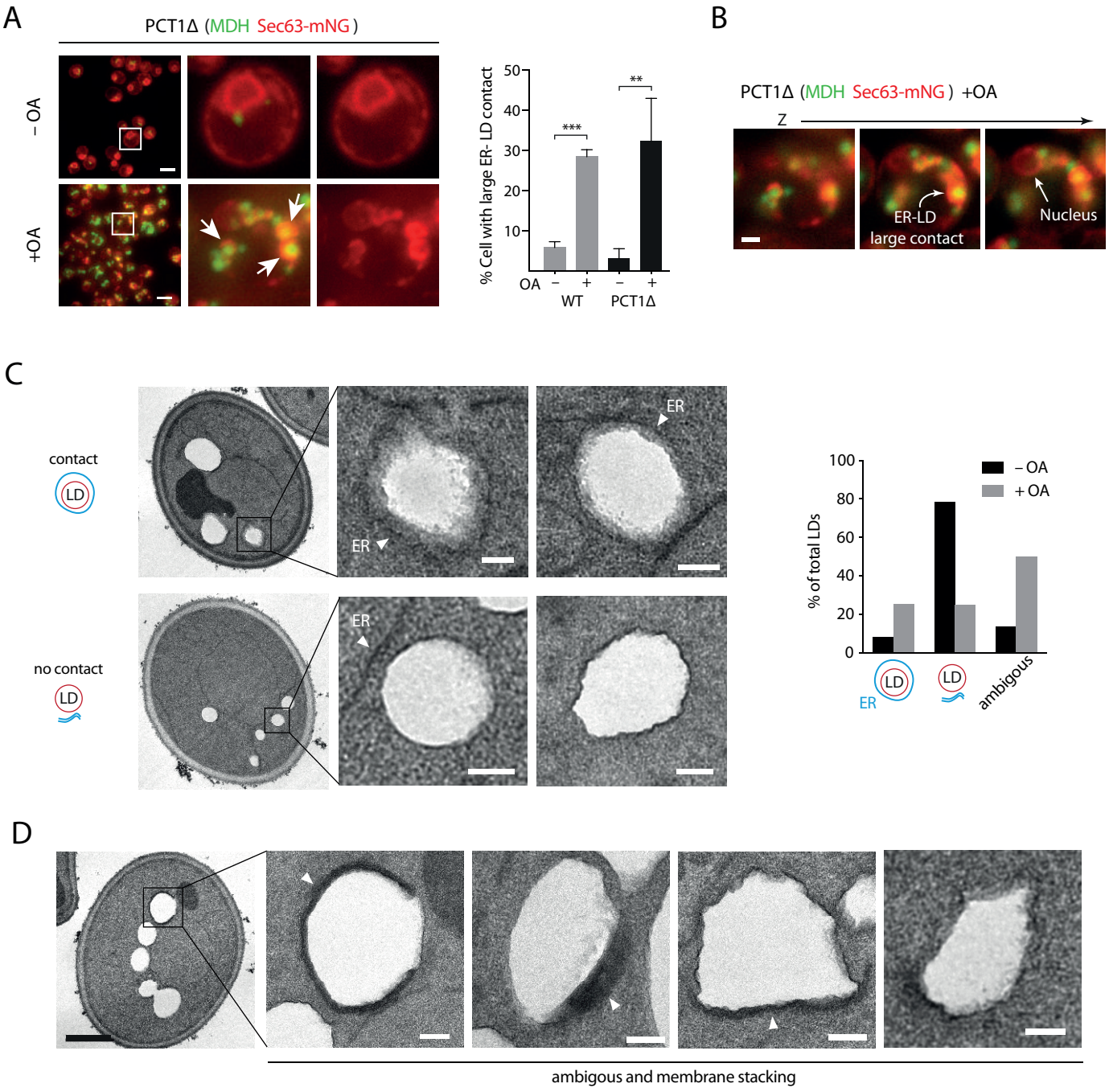
A
PCT1Δ (MDH Sec63-mNG)
– OA
+OA
% Cell with large ER- LD contact
50
40
30
20
10
***
**
OA – + – +
WT
PCT1Δ
B
PCT1Δ (MDH Sec63-mNG) +OA
Z
ER-LD
large contact
Nucleus
C
contact
LD
no contact
LD
ER
ER
ER
ER
% of total LDs
100
80
60
40
20
0
– OA
+ OA
LD
ER
LD
ambigous
D
ambigous and membrane stacking

Supplementary Figure S4 | Complementary microscopy images showing LDs retained in the ER in *Saccharomyces cerevisiae* cells, related to Figure 4

A) PCT1-depleted *Saccharomyces cerevisiae* cells cultured from logarithmic growth phase with and without oleate (OA) treatment. Cells treated with OA show LDs with large ER contact zones (see arrows). Sec63-mNG marks ER and LD are MDH stained. Scale bar is 5 µm. Quantification with WT control is shown on the left. N >100 cells for each condition; Data are represented as mean ±SD.

B) Z-stack corresponding to Z projection displayed in A (PCT1-depleted +OA). Arrows indicates nucleus and large ER-LD contact zone. Scale bar is 1 µm.

C) Left: EM, chemically fixated WT *Saccharomyces cerevisiae* cells treated with OA showing examples of LDs with ER surrounding them (contact) and LDs presenting no apparent ER contact (no contact). Scale bar are 200 nm. Right: quantification of ER-LD contact with and without OA treatment corresponding to condition shown on the left and in Figure 4D. N= 200 LDs. Right: example of categories quantified on the left (contact, no contact and ambiguous).

D) EM, chemically fixated WT *Saccharomyces cerevisiae* cells treated with OA presenting LDs with ambiguous ER contact and unusual membrane stacking surrounding them (see white arrowheads). These phenotypes are not seen in cells without OA treatment. Scale bar are 200 nm.

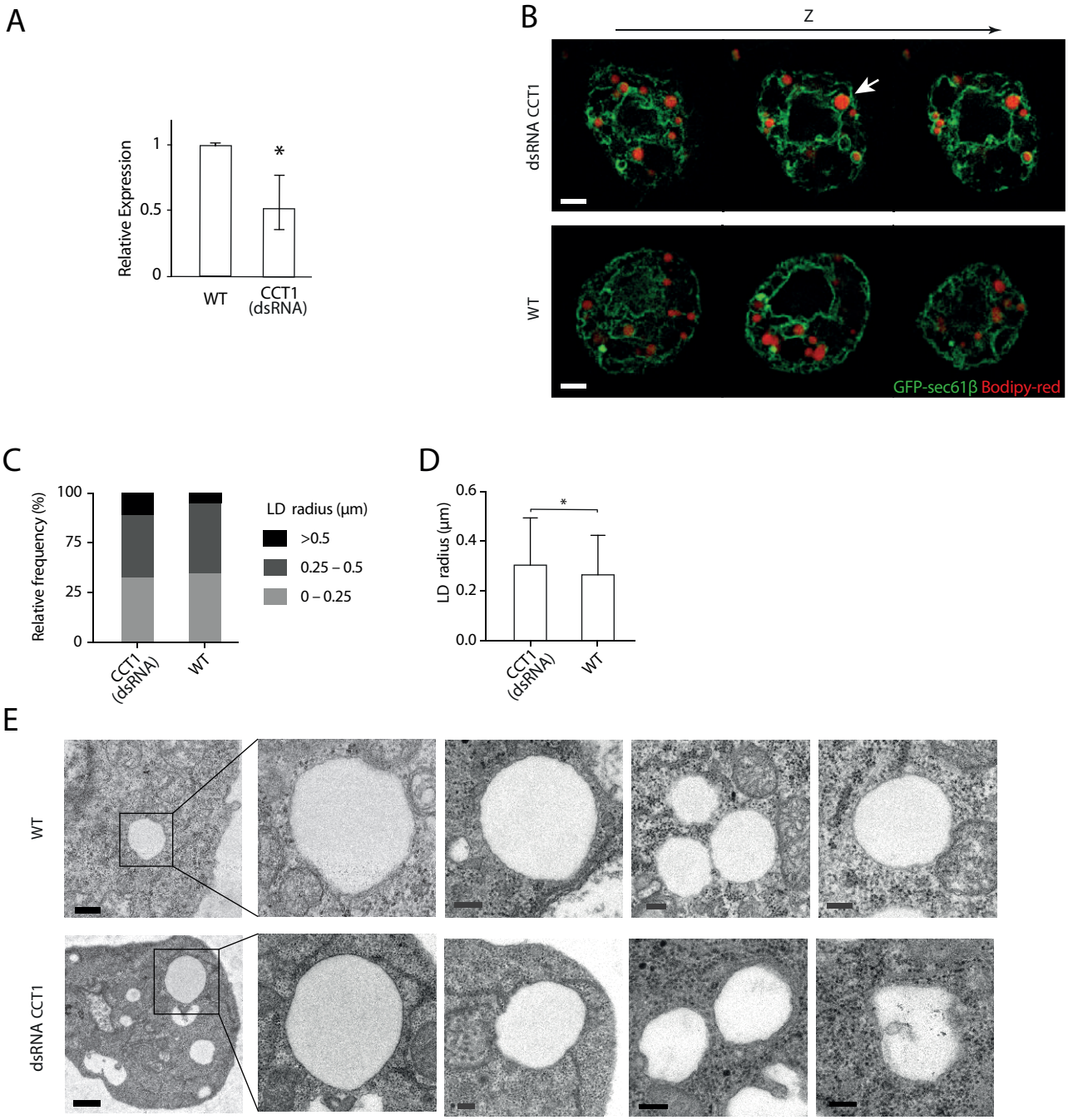
A
Relative Expression
1
0.5
0
*
WT
CCT1 (dsRNA)
B
Z
dsRNA CCT1
WT
GFP-sec61β Bodipy-red
C
Relative frequency (%)
100
75
25
0
LD radius (μm)
>0.5
0.25 – 0.5
0 – 0.25
CCT1 (dsRNA)
WT
D
LD radius (μm)
0.6
0.4
0.2
0.0
*
CCT1 (dsRNA)
WT
E
WT
dsRNA CCT1

Supplementary Figure S5 | Complementary microscopy images showing LDs retained in the ER in *Drosophila* cells, related to Figure 5

A) Quantification of the relative expression of CCT1 in WT and dsRNA CCT1 cells. P-value 0.034 by a permutation test. Data are represented as mean ±SD.

B) Additional z stacks images of Drosophila cells depleted from CCT1 by dsRNA. WT is shown as a control. LDs are induced by oleate and labeled by BODIPY558/568 and GFP-sec61β marks the ER. Arrow points to examples of LDs in close contact with ER. Scale bar is 2 μm.

C) LD radius frequency distribution of droplets smaller than 0.25μm, between 0.25μm and 0.5μm and above 0.5μm displayed for CCT1 depleted and WT Drosophila cells.

D) LD radius of CCT1 depleted and WT Drosophila cells. t-test show ns difference between CCT1 condition and significant difference between depleted cells and WT (p=0.0172). Data are represented as mean ±SD.

E) Example of EM images of LDs in WT and CCT1 depleted cells used for quantification in Figure 5B. Scale bars are 1 μm and 200 nm for the insets.

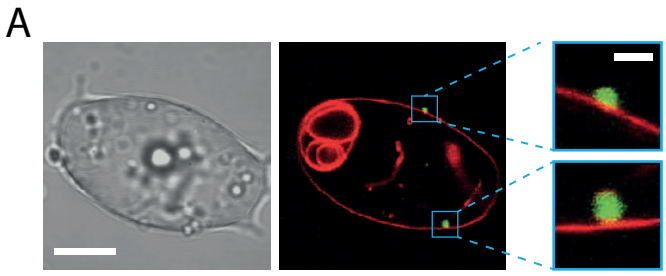
A

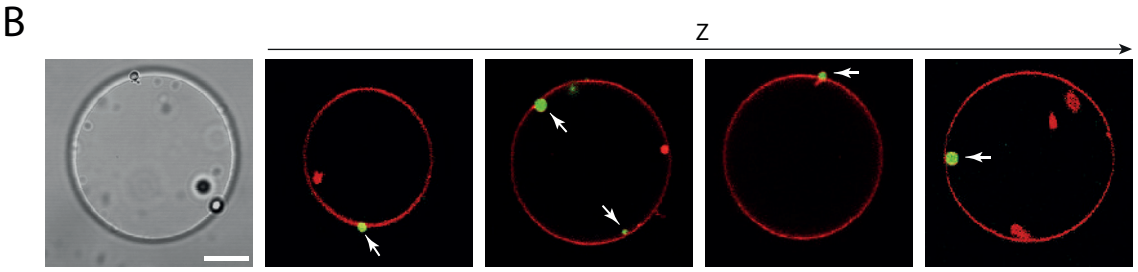
B
z

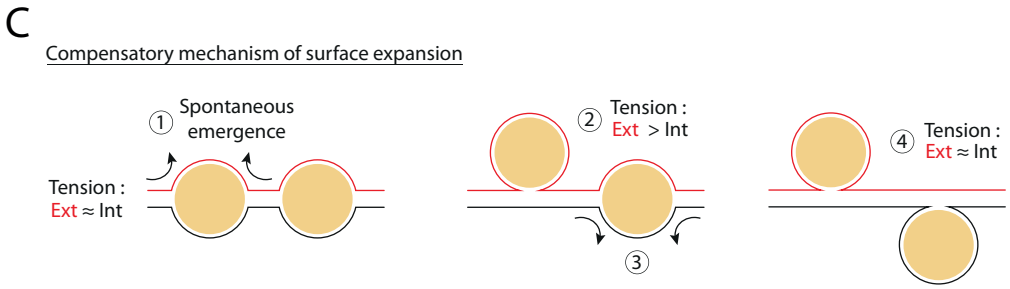
C
Compensatory mechanism of surface expansion
① Spontaneous emergence
Tension : Ext ≈ Int
② Tension : Ext > Int
③
④ Tension : Ext ≈ Int

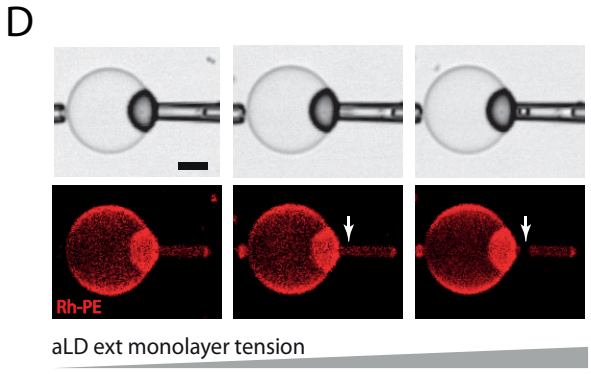
D
Rh-PE
aLD ext monolayer tension

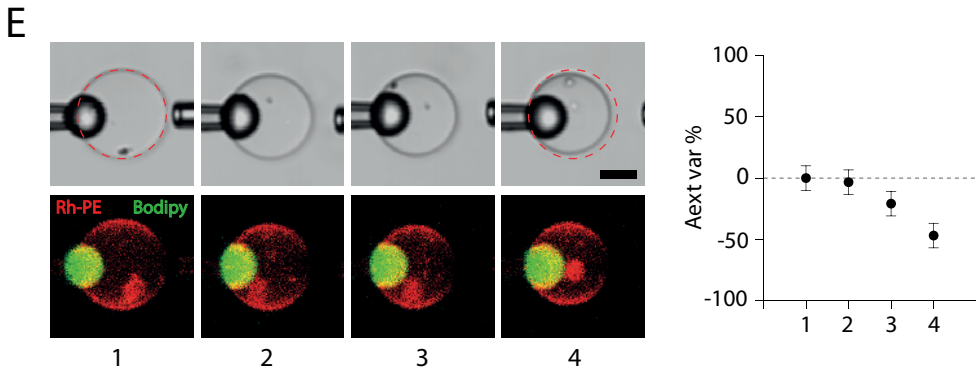
E
Rh-PE
Bodipy
1
2
3
4
Aext var %
100
50
0
-50
-100

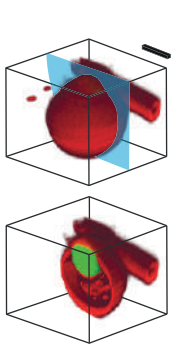
F

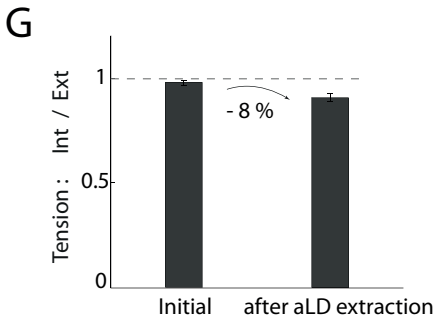
G
Tension : Int / Ext
1
0.5
0
- 8 %
Initial
after aLD extraction

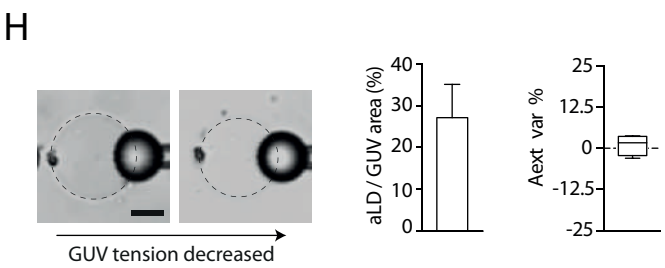
H
GUV tension decreased
aLD / GUV area (%)
40
30
20
10
0
Aext var %
25
12.5
0
-12.5
-25

Supplementary Figure S6 | Detailed examples and model for the compensatory mechanism of the leaflet mismatch by LD emergence, related to Figure 6

A) Non-spherical GUV after strong osmotic deflation (very low bilayer tension) showing externally and internally budded LDs on the same bilayer. Scale bar is 10 µm and 2,5 µm in the inset.

B) Z slices of a GUV with multiple small LDs emerged towards the interior and exterior of the GUV (see arrows). Scale bar is 10 µm.

C) Predicted emergence steps of LDs in a single GUV: (1) at low bilayer tensions spontaneous emergence of an LD, for instance, on the external side of the bilayer; (2) the increase of the external leaflet surface area causes an increase of the external monolayer tension because the amount of phospholipid is constant; (3) the next LD will consequently bud on the opposite side of the bilayer; (4) the internal and external tensions tend to re-equilibrate.

D) Example of the scission of oil tongue describing the ablation of an artificial LD part (Figure 6E). Scale bar is 10 µm.

E) Time lapse of the osmotic deflation of Figure 5E experiment and corresponding LD external area variation showing the internal emergence of the aLD (trapped). Error bars are measurement precision. Scale bar is 10 µm.

F) 3D reconstruction of the final state after osmotic deflation (up) and cross section of the same system. The red cylinder in the background is the glass micropipette. Scale bar is 10 µm.

G) Variation of internal over external monolayer tensions ratio, before and after ablation of an artificial LD piece.

H) Left: A DEV with a ratio of artificial LD/GUV area (middle) close to the one in (Figure 6E) is deflated by osmotic choc. No significant external or internal area variation is observed after osmotic deflation; N = 10. Scale bar is 10 µm. Data are represented as mean ±SD.